Geochimica et Cosmochimica Acta 348 (2023) 239–257

Contents lists available at ScienceDirect

Geochimica et Cosmochimica Acta

journal homepage: www.elsevier.com/locate/gca

Geochemical conditions regulating chromium preservation in marine sediments

S. Bruggmann [a,b,*], S. Severmann [a], J. McManus [c]

[a] Rutgers University, Department of Marine and Coastal Sciences, 71 Dudley Road, New Brunswick, New Jersey 08901, USA
[b] University of Lausanne, Institute of Earth Sciences, Quartier UNIL Mouline, 1015 Lausanne, Switzerland
[c] Bigelow Laboratory for Ocean Sciences, 60 Bigelow Drive, East Boothbay, Maine 04544, USA

ARTICLE INFO

Article history:
Received 24 March 2022
Accepted 1 March 2023
Available online 6 March 2023
Associate editor: Noah J. Planavsky

Keywords:
Continental margin
Early diagenesis
Redox
Bioproductivity

ABSTRACT

In the marine sediment record, concentrations and isotope ratios of chromium (Cr) can be used to reconstruct ocean biogeochemical conditions. These reconstructions rely on a detailed understanding of the chemical pathways that Cr undergoes as it is transferred from the water column to the sediment record. We examined Cr concentrations in marine pore fluids and sediments from six continental margin sites, which can be grouped into two basic environments: (1) sites where sediments are oxygenated and rich in solid phase Mn (herein termed oxic), and (2) sites where sediments are organic C (C_{org})-rich and oxygen is depleted (anoxic). We found Cr concentrations to be lower (maximum of 12 nM in pore fluids and 124 ppm sediment solid phase) at oxic sites compared with anoxic sites (maximum of 77 nM and 184 ppm). Our findings confirm previously published interpretations of dissolved Cr in pore fluids (Brumsack and Gieskes, 1983; Shaw et al., 1990). In oxic surface sediments, particulate Cr(III) can be oxidised by Mn oxides, which leads to elevated concentrations of dissolved Cr co-occurring at the same depth as elevated Mn concentrations in the sediment. Under these oxidising conditions, down-core sediments contain relatively low solid-phase Cr concentrations. In oxic sediments, Cr speciation reveals that most of the pore fluid Cr is in the Cr(VI) state. At the site where Mn oxide-rich sediments rest below an oxic water column, oxidative loss of Cr from the sediment to the bottom water leads to the lowest estimated Cr burial efficiency of the sites examined here. Under anoxic C_{org}-rich conditions, both pore fluids and sediment solid phases contain high Cr concentrations, with 40–80% of dissolved pore fluid Cr present as Cr(III). This enrichment of Cr appears to be tightly linked to the presence of high total organic carbon (TOC) content and scavenging of Cr by (organic) particles in the water column. Combined, these data highlight the strong dependence of Cr on both sedimentary redox conditions as well as biological productivity. Based on the data from modern continental margin sediments, we propose that Cr concentrations and isotope compositions of the authigenic sediment fraction may record a combination of redox conditions and biological productivity in the water column. If confirmed by Cr isotope analyses, these findings will add support for the notion that Cr may serve as a proxy for ocean biological and chemical sedimentological conditions. Thus, careful assessment of the impact of organic matter on Cr is required for reconstructions of redox conditions with sedimentary records.

1. Introduction

Concentrations and isotope compositions of the metal chromium (Cr) in marine environments are sensitive to changes in redox conditions and are also linked to organic carbon (C_{org}) cycling. Since changes in Cr concentrations and isotope compositions may be responsive to biogeochemical conditions in both the water column and sediment, they may be used to reconstruct past ocean conditions, provided that the primary signature is well-preserved in the sediment, and not overprinted by diagenesis. A detailed understanding of Cr cycling in modern marine environments is thus imperative for the utility of such reconstructions.

In modern seawater, Cr occurs as a trace metal at concentrations of nanomoles per litre (e.g., Elderfield, 1970; Cranston and Murray, 1978). Chromium undergoes oxidation–reduction reactions under the conditions commonly encountered in marine environments. The oxidised Cr species, the oxyanion Cr(VI), is soluble and is the thermodynamically favoured Cr species in oxygenated

* Corresponding author at: University of Lausanne, Institute of Earth Sciences, Quartier UNIL Mouline, 1015 Lausanne, Switzerland.
E-mail addresses: sylvie.bruggmann@unil.ch (S. Bruggmann), silke@marine.rutgers.edu (S. Severmann), jmcmanus@bigelow.org (J. McManus).

https://doi.org/10.1016/j.gca.2023.03.003
0016-7037/

seawater (Elderfield, 1970). Under suboxic or anoxic conditions, Cr (VI) can be reduced to the less soluble Cr(III) by reductants such as Fe(II), H_2S, organic compounds or microorganisms (e.g., Pettine et al., 1998; Kim et al., 2001; Ellis et al., 2002a, 2002b; Døssing et al., 2011; Jamieson-Hanes et al., 2012; Kitchen et al., 2012; Basu et al., 2014; Bauer et al., 2018; Nasemann et al., 2020; Joe-Wong et al., 2021). The reduced Cr(III) can contribute over 50% of the total dissolved Cr in oxygen-depleted seawater (e.g., Cranston and Murray, 1978; Rue et al., 1997; Huang et al., 2021). Further, Cr(III) is particle-reactive and is readily removed from the dissolved Cr pool by sorption (e.g., Cranston and Murray, 1978). Re-oxidation of Cr(III) in marine environments can be catalysed by MnO_2, by H_2O_2 or via photooxidation (e.g., Bartlett and James, 1979; Pettine et al., 1991; Liu et al., 2020; Miletto et al., 2021).

Chromium's vertical distribution in the marine environment has a nutrient-type pattern, but this characteristic is less pronounced as compared to other biologically active metals (e.g., Campbell and Yeats, 1984). Even though Cr is not bioessential, Cr can be associated with biological activity (e.g., Jeandel and Minster, 1987; Janssen et al., 2020). In the surface ocean, Cr can be removed from solution onto organic particles (e.g., Semeniuk et al., 2016; Janssen et al., 2021). Rather than being incorporated into organisms, Cr's distribution appears to be dominated by adsorption onto phytoplankton (Wang et al., 1997; Semeniuk et al., 2016).

While cycling of other trace metals, such as Ni, is linked to the cycling of Mn, Cr appears to adsorb inefficiently to Mn oxides (e.g., Shaw et al., 1990). Instead, insoluble Cr(III) is catalytically oxidised by Mn oxides and this oxidation is pH dependent with less oxidation at higher pH values (Fendorf et al., 1992). Nevertheless, provided the solution is supersaturated with respect to Cr(III), Cr hydroxide ($Cr(OH)_3{\cdot}nH_2O$) can precipitate on the surface of Mn oxides (Fendorf, 1995). However, such a precipitate can inhibit further Cr oxidation since Cr(III)(oxyhydr)oxide reacts more slowly with Mn oxides compared with dissolved Cr(III) (Miletto et al., 2021), and these oxides can create a physical barrier between the remaining reduced Cr(III) and the Mn oxide surface (Fendorf et al., 1992). Furthermore, recent incubation experiments showed that microbial Mn(II) oxidation can be coupled to Cr(III) oxidation in marine environments (Miletto et al., 2021).

Under reducing conditions, Cr is accumulated in the sediment due to the poor solubility of reduced Cr(III), and thus, the sedimentary record shows increased Cr concentrations in sediments deposited under anoxic as compared to oxic conditions (e.g., Reinhard et al., 2014). In addition, Cr accumulation within the sediment package is linked to the accumulation of biological material (e.g., recently reviewed by Horner et al., 2021). Enhanced preservation of organic matter under anoxic conditions further fosters elevated Cr concentrations in anoxic C_{org}-rich sediments as compared to oxic C_{org}-poor sediments (e.g., Gueguen et al., 2016; Bruggmann et al., 2019).

While the number of studies on the behaviour of Cr and its isotopes in seawater and in sediments is increasing, information on Cr variations in pore fluids remains scarce. In 1983, Brumsack and Gieskes observed that dissolved Cr concentrations in pore fluids increased with depth due to complexation of Cr with organic matter. At stations on the California and Mexico continental margin with oxygenated surface sediments, distinct peaks in dissolved Cr concentrations up to approximately 85 nM were observed at the sediment–water interface, or at the redox boundary within the sediment (Shaw et al., 1990). These peaks indicate that Cr is released from the solid to the dissolved phase, and can be effluxed to the bottom water. Shaw et al. (1990) suggest that solid-phase Cr (III) – likely associated with biogenic particles – is oxidised by Mn oxides to more soluble Cr(VI). These authors suggest that the deepening of the oxygen penetration depth shortly before sample collection likely caused the dissolved Cr peaks at the redox boundary. Due to the lack of release of dissolved Cr in the Mn reduction zone, Shaw et al. (1990) proposed that Cr sorption onto Mn oxides is less efficient than, for example, for Ni. Further, at sediment depths where chemical conditions are sufficiently reducing, Cr was found to be preserved in the sediment in its reduced form. More recently, Janssen et al. (2021) contributed new dissolved Cr concentration data from pore fluids in carbonate-rich (>70%) sediments. The concentrations in these pore fluids range up to nearly 50 nM and are thus similar to the ones observed by Shaw et al. (1990).

Elevated deep water Cr concentrations gave reason to suggest that a benthic Cr flux contributes Cr from the sediment to the water column (e.g., Jeandel and Minster, 1987). The benthic flux, which is directed out of the sediment as indicated by the negative sign, was estimated to be approximately -3 nmol cm^{-2} y^{-1} for a carbonate-rich station in the Tasman Basin (Janssen et al., 2021). This benthic flux is larger than the model-based estimate of a global benthic flux of -0.1 to -0.2 nmol cm^{-2} y^{-1} as suggested by Pöppelmeier et al. (2021). The differences between the two flux estimates may arise because the benthic Cr flux identified in the Tasman Basin may represent a local, rather than a global value, or because of processes that are under-constrained in the model, such as redox reactions, scavenging by particles, or release from sediments (Janssen et al., 2021; Pöppelmeier et al., 2021).

In addition to variations in Cr concentrations, which can provide insights into biogeochemical changes, Cr isotope compositions (expressed as $\delta^{53}Cr$) can reveal further details about the controls on Cr behaviour. Reduction of Cr(III) to Cr(VI) induces the most prominent Cr isotope fractionation, whereby isotopically light ^{52}Cr is preferentially reduced compared with ^{53}Cr (e.g., Ellis et al., 2002a, 2002b). While global seawater $\delta^{53}Cr$ values typically fall on a global array with an isotope fractionation factor of $-0.8‰$, the factors driving this distribution are not fully understood (e.g., Goring-Harford et al., 2018; Moos and Boyle, 2019; Nasemann et al., 2020; Janssen et al., 2020; Huang et al., 2021).

In this study, we contribute new data on Cr behaviour within marine sediments from sampling sites with a range of redox conditions, Mn and C_{org} concentrations. To identify early diagenetic processes that affect Cr cycling, we examined two characteristic types of environments in detail: (a) C_{org}-poor oxic conditions (termed "oxic") with abundant Mn oxides, and (b) C_{org}-rich reducing (termed "anoxic") conditions. These environments allow assessments of the roles of Mn oxides as catalysts for Cr oxidation, and of organic matter as a net source of Cr to marine sediments. Our data set includes Cr concentrations and redox speciation in pore fluids, concentrations in bulk sediments and sequential extractions. While for some of the stations studied here, Cr concentration data are available (e.g., Shaw et al., 1990), we re-interpret these data in the context of new findings on the marine Cr cycle. This study adds new constraints on Cr biogeochemical cycling at the water–sediment boundary under oxic and anoxic conditions, which aid in describing the pathway of Cr from the water column to the sediment. In return, these insights provide information required to decipher the marine Cr cycle, which can improve interpretations of Cr data from the geological record.

2. Materials and methods

2.1. Sampling sites

We investigate stations located within the upwelling zone along the California and Mexico continental margins (Fig. 1). These sampling sites span a range of bottom water oxygen (O_2) concentrations, C_{org} burial rates, and depths of the Mn and Fe reduction

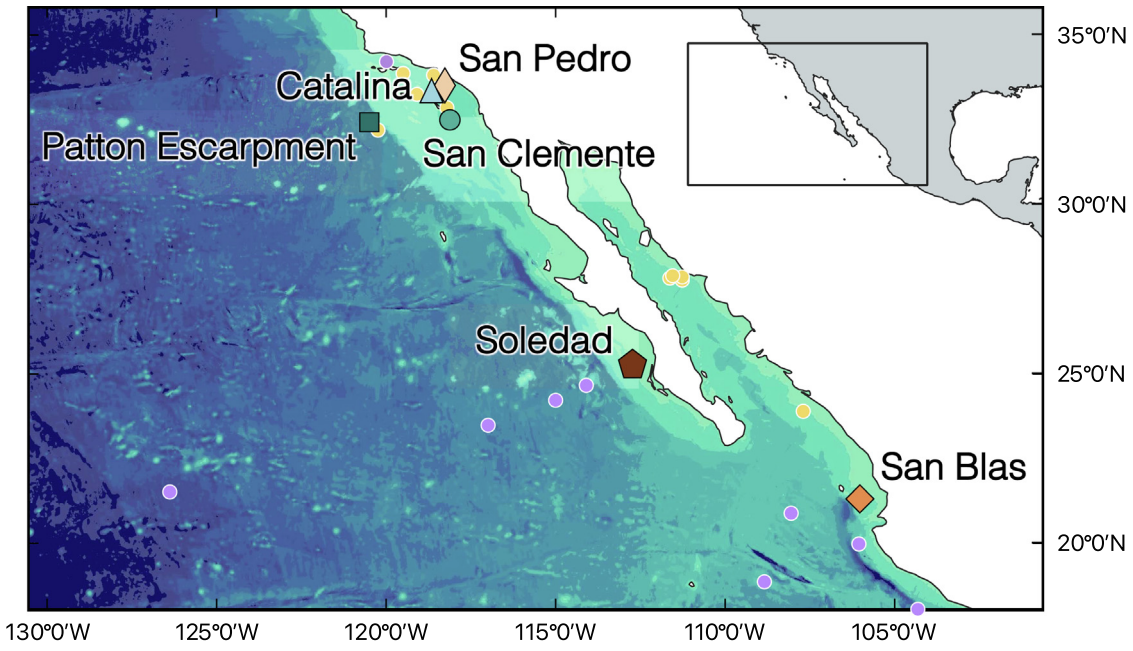

Fig. 1. Map of sampling sites. The map indicates the location of the sampling sites (large symbols; GEBCO Compilation Group (2020) GEBCO 2020 Grid). Stations with high C_{org} burial rates (Soledad, San Blas and San Pedro) are illustrated with brown colours, and sites with more oxic bottom water conditions and low C_{org} burial rates (Patton Escarpment, San Clemente and Catalina) are illustrated in turquoise to blue colours. The small circles with white outlines indicate the sampling sites where previous studies investigated Cr in pore fluids (yellow circles; Brumsack and Gieskes, 1983; Shaw et al., 1990) and the water column (lilac circles; Murray et al., 1983; Moos et al., 2020; Huang et al., 2021).

zones (Table 1). At these sites, oceanographic and geochemical conditions have been well characterised in previous studies (e.g., Berelson et al., 1987; Shaw et al., 1990; McManus et al., 2006a, 2006b; Chong et al., 2012; McManus et al., 2012). In addition, Shaw et al. (1990) presented Cr concentration data in sediments and pore fluids for two of the same stations (Patton Escarpment and San Clemente). For the three oxic stations with bottom water oxygen of 19 μM or higher (Patton Escarpment, San Clemente and Catalina; Fig. 1) turquoise to blue colours are used. The three stations with C_{org} burial rates of $\geq$2.6 nmol m^{-2} d^{-1} and bottom water oxygen of $\leq$8 μM (San Pedro) or <0.1 μM (San Blas and Soledad) are illustrated using brown colours.

The sites located in the Southern California Borderlands (Catalina Basin, San Clemente Basin, Patton Escarpment and San Pedro Basin) underlie the California current system (McManus et al., 1997). The oxygen minimum zone (OMZ) of the Eastern Tropical North Pacific extends between 500 and 1000 m water depth (McManus et al., 1997). Topographic ridges and sills form several submarine basins, where water and chemical exchange is restricted and unique hydrographic conditions are created in each basin (e.g., Sholkovitz, 1972; Berelson et al., 1987; Shaw et al., 1990). Depending on the depth of the sill relative to the OMZ, as well as O_2 consumption within the sediment or bottom water, bottom water O_2 concentrations in the basins are low but variable (Berelson et al., 1987; McManus et al., 1997; Shaw et al., 1990). The Patton Escarpment is the only site that is not located within a silled basin, and is below the OMZ. Collectively, these conditions lead to a range of bottom water O_2 concentrations between 3 and 130 μM, with C_{org} burial rates between 0.08 and 2.6 mmol m^{-2} day^{-1} (Berelson et al., 1996; McManus et al., 2006a, 2006b). At the Catalina Basin, San Clemente Basin and the Patton Escarpment sites, the oxygen penetration depth is ≈0.3 cm, ≈1.3 cm and ≈2.9 cm, respectively (Table 1; Fig. 1; Berelson et al., 1996 and references therein). At the San Clemente and Patton Escarpment sites, the deeper penetration of dissolved O_2 causes a pronounced solid-phase Mn enrichment in the near-surface sediments (McManus

Table 1
Oxygen concentrations, C_{org} burial and mass accumulation rates.

Station		°N	°W	Water depth[a] m	BW O_2[a] μM	O_2 penetration[b] cm	C_{org} burial[a] mmol m^{-2} d^{-1}	MAR[c] mg cm^{-2} y^{-1}
Patton Escarpment	US	32.4	120.6	3707	132	2.20 to 2.87	0.08	3
San Clemente	US	32.6	118.1	2053	52	0.63 to 1.28	0.9	15
Catalina	US	33.3	118.6	1300	19	0 to 0.61	1.2	14
San Pedro	US	33.5	118.4	896	3 to 8	0 to 0.16	2.6	29
San Blas	MX	21.3	106	430	<0.1	0	3.2	21
Soledad	MX	25.2	112.7	542	<0.1	0	8.4	50

Data on oxygen concentrations, C_{org} burial and mass accumulation rates are presented for the sites investigated here.
[a] BW = bottom water; McManus et al. (2006a, 2006b).
[b] Berelson et al. (1996); McManus et al. (2005); Chong et al. (2012).
[c] MAR = sediment mass accumulation rate; McManus et al. (2006a, 2006b); Poulson et al. (2006).

et al., 2006a, 2006b). At the Mexican sites, oxygen penetration is insignificant, and near-surface Mn oxide enrichments were therefore absent.

The Mexican sites, Soledad and San Blas, are located within the Eastern Tropical North Pacific OMZ (see McManus et al., 2006a, 2006b and references therein). The sites are characterised by anoxic bottom water (O_2 concentrations below limit of detection (LOD) of 0.1 μM; McManus et al., 2006a, 2006b). In addition, the C_{org} burial rates are high (8.4 and 3.2 mmol m^{-2} day^{-1}, respectively; McManus et al., 2006a, 2006b). In sediments at Soledad, dissolved H_2S concentrations increase with depth (6.9 μM close to the sediment–water interface, 42 μM at 9.5 cm sediment depth; Fig. 1; Chong et al., 2012). Near the sediment surface at the Soledad site, dissolved Fe concentrations are high, but decrease with depth. By 8 cm sediment depth, the dissolved Fe concentrations reach a minimum, whereas sulfide concentrations start to increase, suggesting Fe removal into pyrite (Chong et al., 2012).

2.2. Sample collection, preparation and total organic carbon analysis

At all stations investigated here, sediment and pore fluid samples were collected with a multi-corer during a research expedition in May/June of 2018. For pore fluid extraction, cores were processed immediately (within 2 hrs) *on board* in a temperature-controlled cold room using 8-cm long Rhizon pore fluid samplers (Rhizosphere Research Products, Wageningen, The Netherlands) attached to acid-cleaned syringes. Rhizon samplers were inserted into pre-drilled sampling holes in the side of the core liners. Core material is assumed to be sealed from atmospheric contamination during sampling and no further isolation is imposed during the sampling process. The porous membrane of the Rhizons has a nominal filter size of ≈0.2 μm. Immediately after extraction of ≈20 ml pore fluid, samples were expelled from the syringes into acid-cleaned LDPE bottles. The depths for Rhizon-sampled pore fluids are presented as the approximate insertion depth of each Rhizon relative to the overlying water. Before storage, all samples were acidified with double-distilled HCl to a pH of ≈1.8.

To collect sediment samples, separately collected cores were sliced in 1 to 2 cm increments on deck. The data are presented as the mid-point of a sediment interval. The sediment samples were frozen in polyethylene freezer bags. Sediment samples were freeze-dried and carefully powdered with an agate mortar and pestle before further treatment. Bottom water samples were collected from a Niskin bottle that was attached to the coring frame at ≈1 m height and triggered upon impact on the seafloor.

The sediment samples were incinerated and dissolved in a mixture of HF and HNO_3, following a standard procedure for marine sediment digestion. After dissolution, some samples contained insoluble Al fluorides. These samples were heated in 12% HNO_3 at 60 °C for 36 h, whereafter the fluorides fully dissolved (Muratli et al., 2012). Freeze-dried samples were further analysed for total organic carbon (TOC) contents using a GVI (now Elementar) Isoprime 1000 with Eurovector EA at Bigelow Laboratory for Ocean Sciences. Uncertainties for the TOC measurements are estimated in two ways for this study. Based on a more recent analytical run, TOC uncertainties are typically better than 0.1% C for lower C_{org} concentration samples. However, given the broad range of C_{org} concentrations, we estimate a maximum precision based on the samples from depths >10 cm from each of the sites. The average uncertainty for the sites is 0.2% C with a range from 0.1 to 0.4% C.

2.3. Pre-concentration of Cr from fluid samples

For samples that were collected for Cr concentration analysis, the Mg hydroxide ($Mg(OH)_2$) coprecipitation method was applied, following e.g., Semeniuk et al. (2016). In this method, ammonium hydroxide (NH_4OH) is added to a fluid sample to raise the pH to >8, which leads to precipitation of $Mg(OH)_2$ due to Mg that naturally occurs in seawater. Along with this process, Cr(III) is removed from the solution by adsorption, while Cr(VI) remains in solution.

For total Cr concentrations, acidified fluid samples (pore fluids, bottom water) were spiked with a single isotope spike (^{53}Cr) and the $Mg(OH)_2$ coprecipitation method was used for pre-concentration of total Cr (now present as Cr(III) since the samples were acidified). Specifically, 5 ml aliquots of the sample were spiked with the single isotope spike and equilibrated for 1 h. Between 0.12 ml and 0.28 ml of 7 M NH_4OH was added to the fluid samples to initiate Mg-hydroxide precipitation. After 1 h, the precipitate was separated from the remaining fluid by centrifugation (5 min at 3900 rpm) and the supernatant was discarded. The $Mg(OH)_2$ pellet containing Cr(III) was then dissolved in 20% HNO_3 and diluted for analysis.

Chromium occurs in both its reduced, Cr(III), and oxidised, Cr(VI), redox state in marine fluids. In addition to the total Cr concentrations, dissolved Cr(VI) was isolated from Cr(III) in seawater samples to identify the relative concentrations of Cr(VI) and Cr(III). To accomplish this distinction, unacidified pore fluid samples were processed *on board* by co-precipitating Cr(III) with $Mg(OH)_2$. The concentrations of Cr species were determined at four of our stations (Soledad, San Blas, San Pedro and San Clemente). Pore fluid samples were treated within 2 h of collection by adding 7 M NH_4OH to 20 ml aliquots of the pore fluids. After 1 h the precipitate was separated from the remaining fluid by centrifugation. The remaining supernatant containing Cr(VI) was decanted into acid-cleaned LDPE bottles and acidified to a pH of ≈1.8, and thus, Cr(VI) was reduced to Cr(III). Chromium contained in these supernatants was then coprecipitated with the same method as total Cr in pore fluids and bottom waters. The concentration of Cr(III) was calculated from measured total Cr and Cr(VI) concentrations. We note that pore fluid samples used for total concentration analyses and for Cr speciation were collected from two individual cores. Thus, the Cr concentration in the aliquot of pore fluids that was used *on board* for speciation of Cr may deviate from the one found in the total concentration aliquot.

2.4. Sequential extractions from sediments

A series of sequential extractions was applied to selected sediment samples from Soledad, San Pedro, Catalina, San Clemente and Patton Escarpment, following the procedure of Huerta-Diaz and Morse (1992) with some modifications. In the first step, approximately 200 mg of freeze-dried sediments were leached with 5 ml of 1 M HCl for 24 h on a shaking table at room temperature to extract trace metals associated with the HCl-leachate fraction (Canfield, 1988). This fraction (hereafter named reactive fraction, or when referring to Cr contained in this fraction, $Cr_{reactive}$) contains Cr and other trace metals associated with oxides, sorbed onto surfaces, or associated with carbonates or phosphate minerals. A similar leaching step was used by previous studies, indicating that Al and Ti concentrations, which are commonly used as indicators of detrital contamination (e.g., Reinhard et al., 2014; Cole et al., 2017; Frank et al., 2020), are typically low (extracting typically <10% of total Cr with 0.5 M HCl; Frank et al., 2020).

The samples were centrifuged (15 min at 3900 rpm) and the supernatant containing the reactive fraction was decanted for analysis. The remaining sediment was washed with Milli-Q (18.2 MΩ cm; MQ), centrifuged again, and the supernatant discarded. In the second extraction step, trace metals associated with organic matter were extracted using H_2SO_4. The assumption is that organically bound trace metals are extracted, while trace metals that coprecipitate or adsorb onto FeS, or form other metal sulfide minerals, remain in the solid phase (Huerta-Diaz and Morse, 1990; Scholz and Neumann, 2007). The H_2SO_4-leaching step was only applied to sediments from two of the organic-rich sites, the Soledad and San Pedro sites, and is hereafter referred to as the organic fraction (or $Cr_{organic}$). In the H_2SO_4-leaching step, 5 ml of concentrated H_2SO_4 was added to the HCl-extraction residue and agitated on a shaking table for 2 h. The samples were centrifuged (15 min at 3900 rpm) and the supernatant was decanted for analysis. The H_2SO_4-leaching step was followed by a washing step with MQ. Finally, sediments from the Soledad and San Pedro sites were leached with 5 ml of concentrated HNO_3 on a shaking table for 2 h to extract trace metals associated with pyrite (Huerta-Diaz and Morse, 1990; Scholz and Neumann, 2007). We acknowledge that a leaching step with HNO_3 attacks sediment fractions other than pyrite, e.g., organic matter, but since Cr associated with organic matter was already extracted with the previous step, we hereafter refer to Cr extracted with HNO_3 as the pyrite fraction (or Cr_{pyrite}). The samples were centrifuged (15 min at 3900 rpm) and the supernatant was decanted for analysis. The extractions were evaporated to dryness, oxidised with aqua regia and diluted with 2% HNO_3 for analysis.

2.5. Concentration analysis

For concentration analyses of Fe and Mn in fluids, the samples were diluted and analysed using an Agilent inductively coupled plasma mass spectrometer (ICP-MS) at Bigelow Laboratory for Ocean Sciences. Fluid samples that were pre-concentrated for Cr concentrations and spiked with a single isotope spike (see Section 2.3) were analysed for their Cr concentrations using a Thermo Fisher iCap collision cell ICP-MS at Rutgers University. Chromium concentrations in fluid samples were calculated using isotope dilution (corrected for mass bias; Sargent et al., 2002). An *in-house* seawater standard and a certified seawater standard (CASS-5) were analysed repeatedly to assess the precision of Cr, Fe and Mn. The *in-house* seawater standard was processed three times, and each of the processed standards were analysed two to three times. In combination, these repeated analyses resulted in a relative standard deviation (RSD) for dissolved Cr, Fe and Mn of ±≤5%. The concentration of dissolved Cr (2.51 nM (±1.5% RSD); n = 3) measured for CASS-5 is slightly higher than the certified value (2.04 nM ± 0.25). For Fe and Mn, the *in-house* seawater standard was spiked with Fe and Mn and repeated analyses (n = 11) resulted in ±≤5% of the expected value.

Solid metal concentrations of dissolved sediment samples (bulk and sequential extractions) were analysed using the iCap ICP-MS Thermo Fisher at Rutgers University. A shale geological standard reference material (SDo-1, Devonian shale) was processed along with each batch of solid samples (including bulk digests and sequential extractions). The shale standard was analysed repeatedly during each session, resulting in an internal reproducibility of ±≤10% RSD (n = 3) for all elements reported here. Repeated bulk digests of the shale standard (n = 3) resulted in ±≤14% RSD. In addition, replicates of three samples that were bulk digested, and two samples that were sequentially extracted resulted in a ±≤17% RSD. Average concentrations of Cr (62.5 ppm), Fe (7.1 wt %), Mn (298.4 ppm) and Al (7.4 wt%) of the shale standard are within the range of published concentrations (e.g., 63.4 ppm (Cr), 6.8 wt% (Fe), 298.9 ppm (Mn) and 6.3 wt% (Al) published by Olson et al., 2019).

2.6. Calculations of benthic fluxes, and burial efficiencies

Estimates of diffusive benthic fluxes of Cr were calculated using Fick's first law of diffusion:

$$benthic\ \ flux = -\phi * D_{sediment} * \frac{d[C]}{dx} \quad (1)$$

with the average porosity (ϕ; values based on McManus et al., 2005) and the concentration gradient from bottom water across the sediment–water interface ($d[C]/dx$). Based on this equation, negative benthic fluxes are directed out of the sediment. For bottom water concentrations, we use the measured bottom water Cr concentrations (Table 2). Notably, the bottom water samples that are used as estimates of the concentrations at the sediment–water interface were collected approximately 1 m above the sediment–water interface. The diffusive boundary layer, however, is on the order of mm, and a vertical offset of the bottom water from the sediment–water interface introduces a large uncertainty (e.g., Lorke et al., 2003). The concentration gradient is estimated as a linear gradient between the bottom water value and the value of the uppermost pore fluid sample (1 to 2 cm sediment depth). Since our bottom water samples were collected 1 m above the sediment–water interface, we calculate an average uncertainty on the order of 50%. This average includes estimated uncertainties in the diffusion coefficient, uncertainties in the depth assignments for the gradient, and the shape of the gradient, i.e., we employ a linear gradient rather than a non-linear fitting function. The diffusion coefficient in the sediment ($D_{sediment}$) was calculated as

$$D_{sediment} = \frac{D_{seawater}}{\theta^2} \quad (2)$$

The diffusion coefficient of CrO_4^{2-} in seawater ($D_{seawater}$ at 25 °C = 11.2 10^{-6} cm^2 sec^{-1}) and of Cr^{3+} in seawater ($D_{seawater}$ at 25 °C = 5.9 10^{-6} cm^2 sec^{-1}) were taken from Li and Gregory (1974). Using the relationship between porosity and tortuosity (θ^2), tortuosity was derived after Boudreau (1996).

$$\theta^2 = 1 - \ln(\phi^2) \quad (3)$$

We note that we exclusively estimate diffusive benthic Cr fluxes, rather than combined diffusive and advective fluxes, which would require incubations with benthic chambers. Lenstra et al. (2020) show that for Fe and Mn, calculated diffusive fluxes can deviate from *in situ* measured fluxes by an order of magnitude in both directions. Because of these uncertainties, we use the calculated benthic Cr fluxes exclusively as estimates.

Published sediment mass accumulation rates (MAR; Table 1; McManus et al., 2006a, 2006b; Poulson et al., 2006) were used to calculate the MAR of Cr (Cr MAR) by multiplying MAR by Cr concentrations averaged over the upper 10 cm of the sediment. Surface peaks of solid-phase Cr could cause an overestimation of Cr MAR. However, the surface peaks in our sediments are too small to affect the Cr MAR (see Section 3). The Cr rain rate was calculated as

$$rain\ \ rate = (-benthic\ \ flux) + MAR \quad (4)$$

and the burial efficiency of Cr was calculated following Berelson et al. (1996) as

$$burial\ \ efficiency = \frac{MAR}{rain\ \ rate} \quad (5)$$

Since the benthic fluxes hold large uncertainties and should be treated as estimates, also the rain rate and burial efficiency should be considered as estimates.

Table 2
Dissolved pore fluid concentrations and speciation of dissolved Cr in pore fluids.

Station	Depth cm	Fe mM	Mn mM	Cr nM	Cr(VI) nM	Cr(III) nM
Patton Escarpment	bottom water			4.21		
	1	0	0.01	9.65		
	2	0	0.02	10.2		
	3	0	0.02	12.3		
	4	0	0.23	9.15		
	5	0.1	1.4	3.70		
	6	0	5.46	1.31		
	7	0	7.22	1.67		
	8	0.1	10.76	1.87		
	9	0.1	8.01	1.47		
	10	0	15.35	1.29		
San Clemente	bottom water			4.08		
	0.5	<LOD	1.4	6.81		
	1.5	<LOD	12.1	3.51	3.69	e
	2.5	<LOD	54.7	1.71		
	3.5	<LOD	47	1.46	2.94	e
	4.5	0.5	67.6	1.56		
	5.5	1.1	69.4	1.84	2.14	e
	7.5	3.5	67	1.37	1.31	0.06
	9.5	6.3	61.2	0.94	1.46	e
	11.5	11	84.6	1.79	1.70	0.09
	13.5	8.8	71.1	1.98		
	15.5	9.9	76.6	1.82	1.94	e
	19.5	8.8		2.32		
	25.5	8.4	84.3	1.91		
Catalina	bottom water			3.26		
	1	<LOD	3.1	3.02		
	2	19.1	7.3	2.43		
	3	27.7	6	2.16		
	4	24.8	3.1	1.81		
	5	16.2	1.7	2.21		
	9	35.9	2.8	2.56		
	13	28.4	2.6	3.16		
	17	19.4	2.2	2.81		
	21	14	2	2.60		
	25	9.5	1.9	2.52		
San Pedro	bottom water			3.02		
	1	33.2	<LOD	3.70		
	2	14.4	<LOD	3.02	1.57	1.45
	4	14	<LOD	2.89	1.77	1.12
	5	74.5	<LOD	6.61	2.60	4.01
	9	87.3	<LOD	7.09	2.83	4.26
	11	78.5	<LOD	6.60	1.85	4.75
	13	64.8	<LOD	5.41	2.60	2.81
	17	69.7	0.2	8.87	4.17	4.70
	19	62.4	0.1	8.73	4.47	4.26
San Blas	bottom water			2.05		
	1	66.1	<LOD	12.1		
	2	76.4	0.1	17.6	4.26	13.4
	3	66.8	0.1	17.2	4.28	13.0
	4	72.5	0.1	19.6	6.20	13.4
	5	70.3	0.2	20.3	6.54	13.7
	7	74	0.2	23.9	9.21	14.7
	9	64.5	0.2	22.7		
	11	53.5	0.2	24.5	10.4	14.1
	13	43.9	0.1	28.2	11.7	16.5
	15	31.8	0.1	29.0	13.5	15.5
	17	19.4	0.1	31.9	12.9	19.0
	19	7.5	0.1	33.8	16.1	17.7
Soledad	bottom water			2.43		
	1	41.8	<LOD	24.9	7.32	17.5
	2	26.4	<LOD	19.5	4.83	14.7
	4	16.4	<LOD	21.7	4.55	17.1
	5	7.3	<LOD	35.3	16.4	18.9
	7	1.8	<LOD	37.4	20.2	17.2
	9	<LOD	<LOD	43.4	13.2	30.2

Table 2 (*continued*)

Station	Depth cm	Fe mM	Mn mM	Cr nM	Cr(VI) nM	Cr(III) nM
	11	0.7	<LOD	56.6	16.1	40.5
	13	<LOD	<LOD	60.4	19.9	40.5
	15	<LOD	<LOD	64.2	30.0	34.2
	17	<LOD	<LOD	70.5	28.6	41.9
	19	<LOD	<LOD	76.5	26.0	50.5

The concentrations of dissolved elements in pore fluids and the speciation of Cr are shown, with LOD for Fe of 0.455 μM, and for Mn of 0.065 μM. While total Cr and Cr(VI) were measured for each sample, Cr(III) concentrations were calculated from the former two values. For a few samples, the measured Cr(VI) exceeds the measured concentration of total Cr. These samples are indicated by the letter "e".

3. Results

3.1. The oxic sites

At the sites having bottom water oxygen of 19 μM or higher (Patton Escarpment, San Clemente and Catalina; Fig. 2), symbols and lines are illustrated in turquoise to blue colours. At these sites, dissolved Cr concentrations in pore fluids were low, ranging between 0.9 nM and 12.3 nM and exceeding the bottom water concentration by a factor of <3 (Fig. 3; Table 2). The highest concentration occurred at the Patton Escarpment site, where dissolved Cr peaked at 3 cm sediment depth, and decreased to concentrations <2 nM below 5 cm sediment depth. At the San Clemente site, the maximum dissolved Cr concentration in pore fluids was found in the surface sediment sample (6.8 nM at 0.5 cm sediment depth). At the Catalina site, dissolved Cr concentrations in pore fluids show a narrow range between 1.8 nM and 3.8 nM. At the San Clemente site, all pore fluid Cr is present as Cr(VI) (Fig. 4; Table 2; note no speciation data for Patton Escarpment). The Cr(VI) concentrations exceeding total dissolved Cr concentrations (Table 2) can be explained by our sampling strategy. Pore fluid samples for total Cr and for Cr speciation analyses were collected from two individual cores. Thus, low concentration variations can arise. Unfortunately, the volume of fluid samples from Patton Escarpment and Catalina Basin were insufficient for speciation analysis. Estimated benthic fluxes of Cr show a negative sign, i.e., they were directed out of the sediment at Patton Escarpment and San Clemente (−0.76 and −0.43 nmol cm^{-2} y^{-1}, respectively; Table 3), with an estimated uncertainty of 50% or more.

The TOC content was lowest in sediments at the oxic stations and generally higher at the more reducing sites (Fig. 2; Table 4). At the Patton Escarpment and San Clemente sites, we observed near-surface peaks in both solid Mn/Al and Cr/Al in total digests, although the Cr/Al peak at San Clemente is small (Fig. 5; Table 4). The maximum sediment Mn concentration occurred at San Clemente ≈23,000 ppm between 0 and 1 cm sediment depth. Sediment Cr concentrations are highest at the Catalina site (up to 124 ppm at 6–7 cm sediment depth; Fig. 5). In addition, the authigenic Cr concentrations presented in the Supplementary Material were calculated from bulk concentrations corrected for detrital

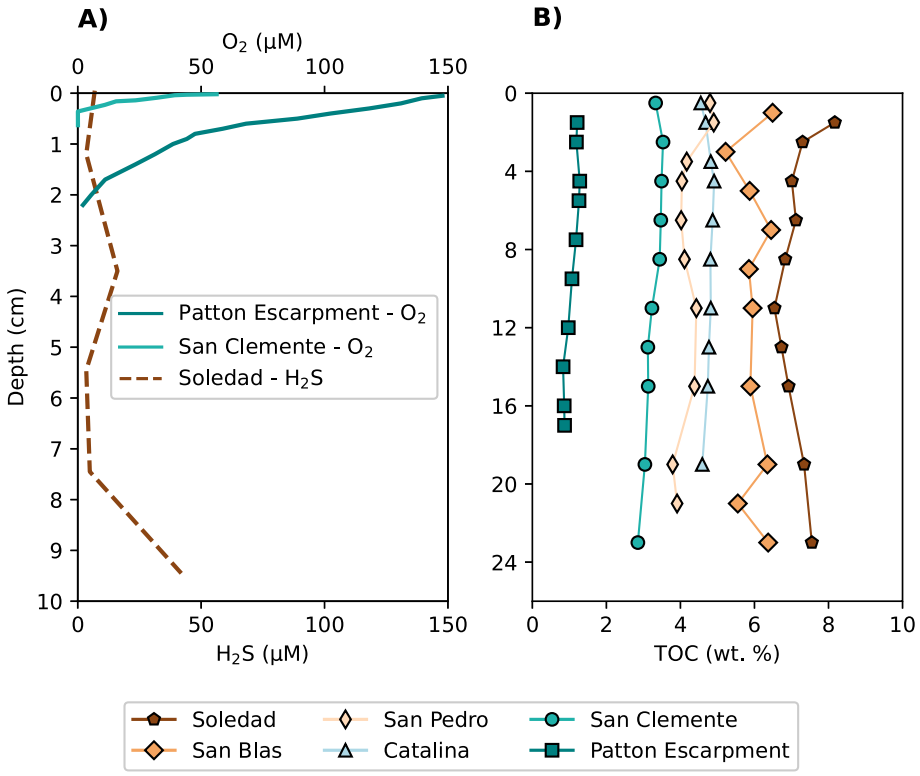

Fig. 2. Chemical parameters. The depth plots show the distribution of (A) dissolved O_2 and dissolved H_2S in pore fluid (Chong et al., 2012), and (B) TOC contents in bulk sediments. The dissolved O_2 and H_2S data were analysed on samples collected before the samples used for this study (see Chong et al. (2012). Note the different scale of (A) and (B).

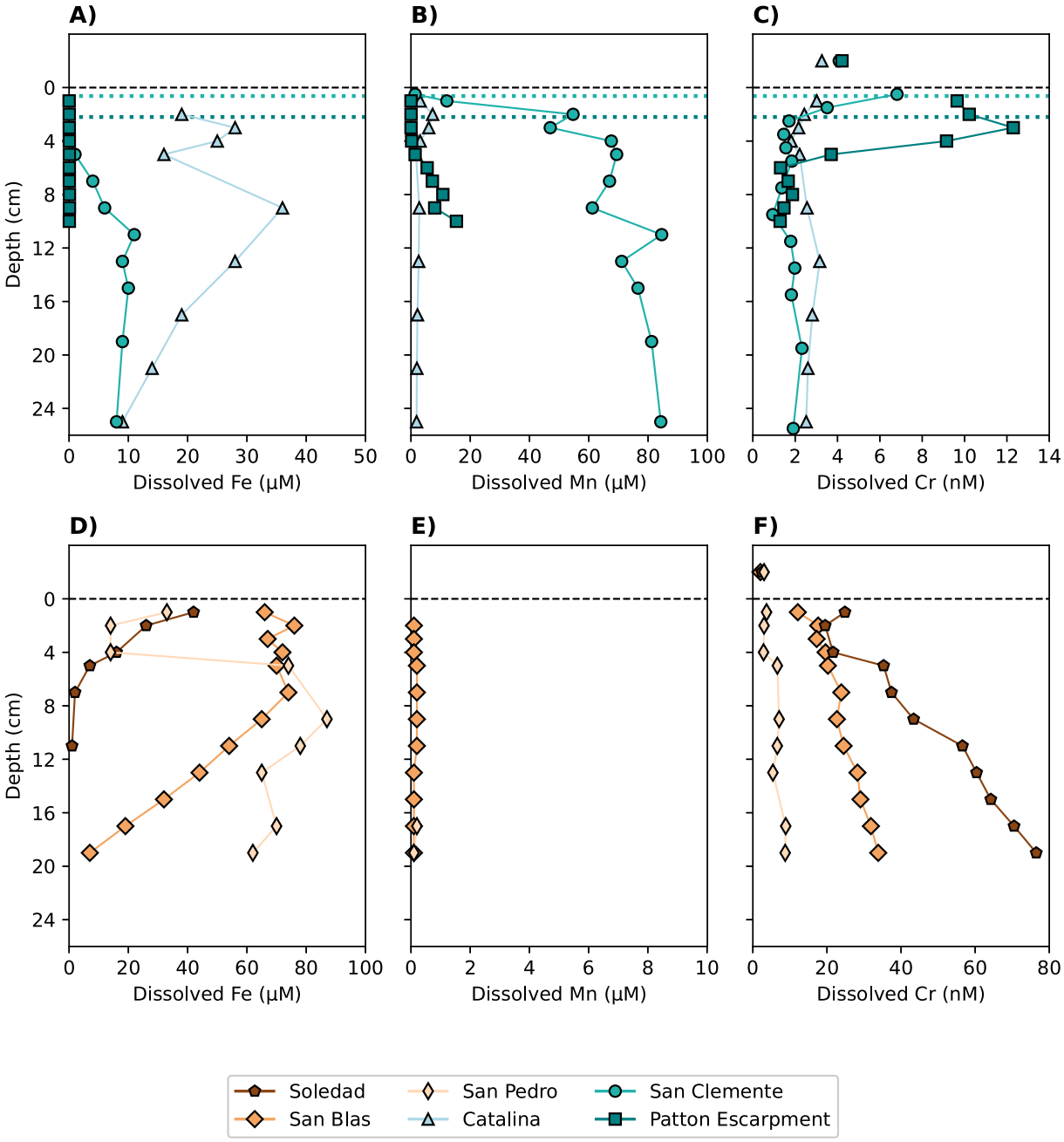

Fig. 3. Dissolved pore fluid concentrations. The depth plots show dissolved concentrations of Fe, Mn and Cr in the pore fluids of oxic (A–C) and anoxic sites (D–F). The horizontal dashed lines (black) indicate the sediment–water interface, and bottom water samples are illustrated above the sediment–water interface (the y-axis above sediment–water interface is not true to scale). Horizontal dotted lines (blue colours) indicate the oxygen penetration depth (Chong et al., 2012).

contamination with estimated detrital Cr/Al ratios (see Frank et al., 2020; Table S1). Chromium concentrations in sequential extracts reveal that the reactive fractions at the Patton Escarpment, San Clemente and Catalina Basins are on average 13.1 ppm (±3.6 SD, n = 30; Fig. 6; Table 5) – lower than the anoxic sites. The concentrations of Ti in the reactive fractions were below detection limit (0.003 ppm).

3.2. The anoxic sites

For the low-oxygen sites with C_{org} burial rates ≥2.6 mmol m^{-2} d^{-1} (Soledad, San Blas and San Pedro), brown colours are used to depict the data points. The dissolved Cr concentrations in pore fluids at these stations increased with depth and were noticeably higher than at the oxic sites, exceeding bottom water concentration by a factor of up to ≈30. (Fig. 3; Table 2). The dissolved Cr concentrations were highest at the Soledad site (76.5 nM at 19 cm sediment depth), where the average TOC content was also highest (≈7.5 wt%). At the anoxic sites, Cr(III) increased with depth (Fig. 4). Between 39 and 79% of the total dissolved Cr in pore fluids is Cr(III). At the Soledad site, the estimated benthic flux of Cr was with −3.60 nmol cm^{-2} y^{-1} negative, i.e., directed from the sediment to the bottom water. At the other two anoxic stations, the benthic flux was also directed out of the sediment (−1.62 nmol cm^{-2} y^{-1} and −0.11 nmol cm^{-2} y^{-1} for San Blas and San Pedro, respectively). We note that these calculations use the diffusion coefficient of Cr

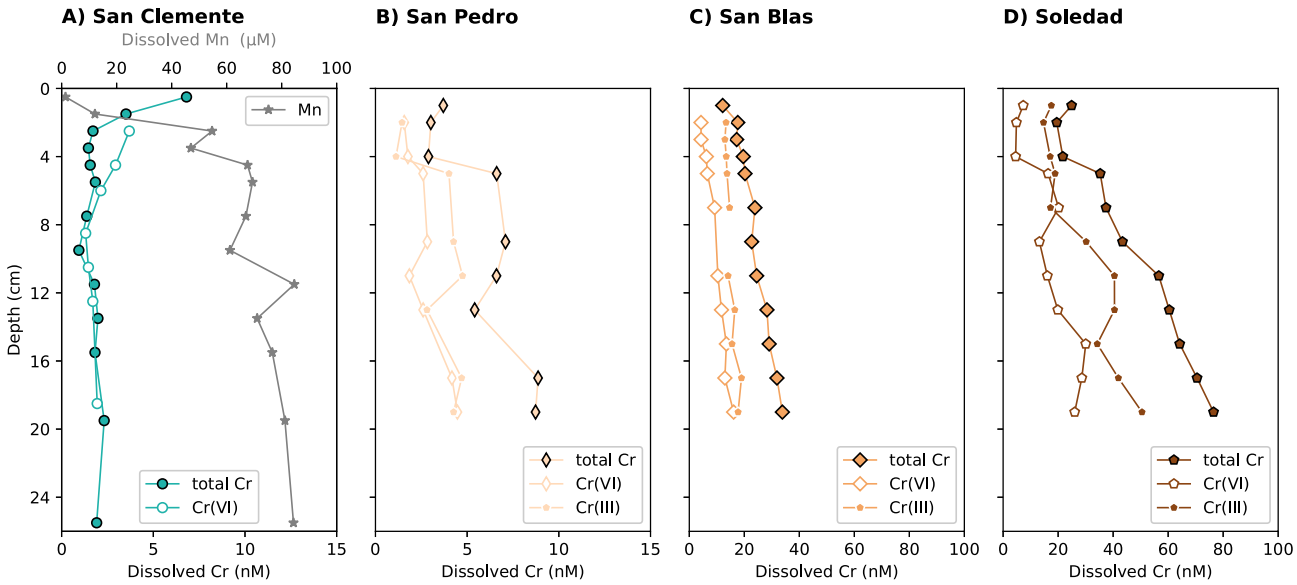

Fig. 4. Speciation of dissolved Cr in pore fluids. The depth plots show Cr speciation in the pore fluids prepared with Mg hydroxide coprecipitation. From the measured concentrations of total dissolved Cr and Cr(VI), Cr(III) concentrations were calculated as the difference between the total Cr and Cr(VI). The Cr(III) concentrations are not plotted in A) since they are close to 0 ppm.

Table 3
Benthic diffusive fluxes, calculated from pore fluid concentrations.

Station	Φ[a]	T °C	$D_{sediment}$[b] 10^{-6} cm^2 sec^{-1}	Flux nmol cm^{-2} y^{-1}
Patton Escarpment	0.93	1.5	4.78	−0.76
San Clemente	0.93	4	5.32	−0.43
Catalina	0.89	4	4.94	0.03
San Pedro	0.94	5	5.63	−0.06
San Blas	0.94	4	5.42	−0.86
Soledad	0.94	4	5.42	−1.91

The diffusive benthic fluxes were calculated from pore fluid concentrations.
[a] McManus et al. (2005), Soledad and San Blas estimated based on McManus et al. (2005).
[b] $D_{seawater}$ at 25 °C for CrO_4^{2-} = 11.2 * 10^{-6} cm^2 sec^{-1} and for Cr^{3+} 5.9 * 10^{-6} cm^2 sec^{-1} (Li and Gregory, 1974).

(VI), even though almost 80% of Cr can be present as Cr(III). We therefore also calculated the estimated benthic fluxes of the anoxic sites using the diffusion coefficient of Cr^{3+} in seawater ($D_{seawater}$ at 25 °C = 5.94 10^{-6} cm^2 sec^{-1}; Li and Gregory, 1974). These results yield estimated benthic fluxes of −1.91 nmol cm^{-2} y^{-1} (Soledad), −0.86 nmol cm^{-2} y^{-1} (San Blas) and −0.06 nmol cm^{-2} y^{-1} (San Pedro), which are used in the discussion of this study (Table 3).

In sediments from the anoxic sites, solid Cr concentrations of total digests reached up to 183 ppm (San Pedro; Fig. 5), but the highest Cr/Al ratio (4.9 * 10^{-3} ppm/ppm) occurs at the Soledad site as observed for the dissolved Cr concentrations in pore fluids (Tables 2 and 4). At the San Blas site, sediment Cr concentrations are lower compared with the San Pedro site (San Blas: 48 to 98 ppm; San Pedro: 111 to 183 ppm). In contrast to this difference, San Blas has a higher TOC content (up to 6.5 wt%) compared with San Pedro (up to 4.9 wt%). Soledad, where the C_{org} burial rate is highest, has the highest TOC contents (up to 8.17 wt%). At San Blas, sediment Al concentrations are elevated compared with the other anoxic stations (with averages of ≈80,000 ppm and ≈42,000 ppm, respectively). The sequential extractions show that at the Soledad site, the reactive fraction contains an average Cr concentration of 40 ppm (≈45%), the organic fraction of 27 ppm (≈33%), and the pyrite fraction of 19 ppm (≈22%; Fig. 6; Table 5). The San Pedro site holds similar Cr concentrations in all leachate fractions (≈20 ppm). As for the oxic sites, Ti concentrations were below detection limit.

4. Discussion

4.1. Chromium cycling under oxic organic-poor conditions

Because of the different solubilities of Cr(III) and Cr(VI), redox conditions are assumed to have an impact on the distribution of Cr in marine environments, and in particular the accumulation of Cr within the sediment package. At the San Clemente Basin and Patton Escarpment sites, dissolution and re-precipitation of Mn oxides result in a solid-phase Mn maximum near the sediment–water boundary, consistent with an active oxidation front (Froelich et al., 1979; Shaw et al., 1990; McManus et al., 2012). Shaw et al. (1990) also measured sediment and pore fluid Cr concentrations in sediments from San Clemente and Patton Escarpment and found that Cr was not released in the Mn reduction zone. Other elements (e.g., Ni, V Co, Mo and Cu) have been demonstrated to sorb onto Mn oxides forming in surface sediments (Shaw et al., 1990). These Mn oxide-associated trace metals tend to have elevated pore fluid concentrations in the Mn reduction zone (i.e., below the solid-phase Mn peak), where they are released back into the pore fluid as their carrier phase dissolves. Thus, Cr's behaviour contrasts with that of other metals, as it seems to be inefficiently sorbed onto Mn oxides (Shaw et al., 1990). Instead, Cr release from the solid to the dissolved phase seems to occur concomitantly with the Mn oxide peak due to catalytic oxidation of insoluble Cr(III) to soluble Cr(VI), which can effectively escape sorption onto Mn

Table 4
Solid concentrations from sediment total digests.

Station	Depth cm		Al ppm	Fe %	Mn ppm	Cr ppm	Cr/Al * 10^{-3} ppm/ppm	TOC wt.%	Cr:C µmol/mol
Patton Escarpment	1	2	47,708	2.9	6031	52.7	1.10	1.21	1006
	2	3	76,591	4.6	10,327	87.9	1.15	1.19	1706
	4	5	81,316	5.0	6729	93.3	1.15	1.28	1684
	5	6	72,795	4.5	5125	83.4	1.15	1.26	1529
	7	8	55,973	3.4	1880	61.5	1.10	1.18	1204
	9	10	73,961	4.5	1375	84.3	1.14	1.07	1820
	11	13	68,709	4.1	743	77.2	1.12	0.97	1838
	13	15	63,886	4.2	513	70.2	1.10	0.83	1954
	15	17	66,588	4.3	481	74.0	1.11	0.86	1988
	16	18	67,196	4.1	488	77.9	1.16	0.87	2068
San Clemente	0	1	21,000	1.5	22,674	54.9	2.62	3.33	381
	2	3	45,845	3.2	11,412	45.6	0.99	3.53	298
	4	5	47,414	3.6	1494	57.3	1.21	3.49	379
	6	7	34,436	2.6	956	27.4	0.80	3.47	182
	8	9	42,164	2.9	1117	49.5	1.17	3.44	332
	10	12	50,781	3.6	1280	67.1	1.32	3.23	480
	12	14	28,341	2.1	600	57.0	2.01	3.12	422
	14	16	63,922	4.5	1220	58.2	0.91	3.13	430
	18	20	53,714	3.9	1032	62.8	1.17	3.04	477
	22	24	47,216	3.4	989	62.6	1.32	2.85	507
Catalina	0	1	59,615	3.9	950	111	1.86	4.55	564
	1	2	59,798	4.1	359	103	1.73	4.68	508
	3	4	70,738	4.3	331	121	1.72	4.82	580
	4	5	65,070	4.0	298	116	1.78	4.91	546
	6	7	69,511	4.2	328	124	1.78	4.87	588
	8	9	71,534	4.1	339	122	1.70	4.81	586
	10	12	70,845	4.2	327	113	1.60	4.82	542
	12	14	62,384	3.8	258	101	1.62	4.77	489
	14	16	63,258	3.7	274	99.9	1.58	4.74	487
	18	20	68,237	4.0	300	106	1.55	4.59	533
San Pedro	0	1	47,920	3.5	337	124	2.59	4.80	597
	1	2	53,983	3.4	363	183	3.38	4.90	863
	3	4	63,464	3.8	408	118	1.86	4.17	654
	4	5	60,054	3.6	374	150	2.50	4.04	858
	6	7	54,071	3.4	361	129	2.39	4.02	741
	8	9	55,649	3.2	368	115	2.07	4.11	646
	10	12	58,192	3.6	392	111	1.91	4.43	579
	14	16	63,450	3.7	395	111	1.75	4.38	585
	18	20	62,057	3.6	399	129	2.08	3.79	786
	20	22	68,071	4.1	446	120	1.77	3.91	709
San Blas	0	1	61,898	3.0	95	73.2	1.18	6.49	260
	2	3	84,559	3.2	162	81.9	0.97	5.22	363
	4	5	89,194	3.3	151	93.0	1.04	5.87	366
	6	7	88,099	3.1	136	96.5	1.10	6.45	347
	8	9	51,025	1.7	22	48.3	0.95	5.85	190
	10	12	80,381	3.1	156	91.1	1.13	5.95	353
	14	16	83,085	2.9	115	90.0	1.08	5.89	353
	18	20	79,765	3.0	166	97.7	1.23	6.35	357
	20	22	94,862	3.3	158	94.8	1.00	5.55	395
	22	24	84,860	3.0	135	90.9	1.07	6.37	330
Soledad	0	1	21,493	1.2	142	81.9	3.81		
	1	2	30,126	1.7	181	94.5	3.14	8.17	269
	2	3	30,919	1.8	182	91.0	2.94	7.30	288
	4	5	26,810	1.5	169	103	3.84	7.01	339
	6	7	28,161	2.0	168	88.9	3.16	7.12	289
	8	9	26,710	1.7	176	97.6	3.65	6.83	331
	10	12	20,866	1.3	131	102	4.87	6.54	360
	12	14	28,333	1.7	179	95.1	3.36	6.73	326
	14	16	27,004	1.8	182	90.3	3.34	6.92	300
	18	20	34,922	2.2	206	109	3.13	7.34	343
	22	24	33,972	2.0	191	105	3.10	7.55	321

Concentration data of total digests of sediments are reported, along with TOC and Cr:C ratios.

oxides (e.g., van der Weijden and Reith, 1982; Eary and Rai, 1987; Shaw et al., 1990; Fendorf, 1995; Banerjee and Nesbitt, 1999; Tang et al., 2014). Tang et al. (2014) demonstrated in laboratory experiments that oxidation of aqueous Cr(III) is greatly enhanced in the presence of biogenic Mn oxides. The implication of this finding is that dissolved Cr in pore fluids would be present as Cr(VI) in the presence of Mn oxides.

Chromium oxidation by dissolved O_2 is slow, but oxidation proceeds much faster when catalysed by Mn oxides (van der Weijden and Reith, 1982; Manceau et al., 1992). Consequently, the loss of soluble oxidised Cr(VI) should be larger in the presence of Mn oxides as compared to its absence, and accumulation rates of Cr in the sediment should be lower. Indeed, the Cr MAR at San Clemente Basin and Patton Escarpment, where Mn oxides are present in

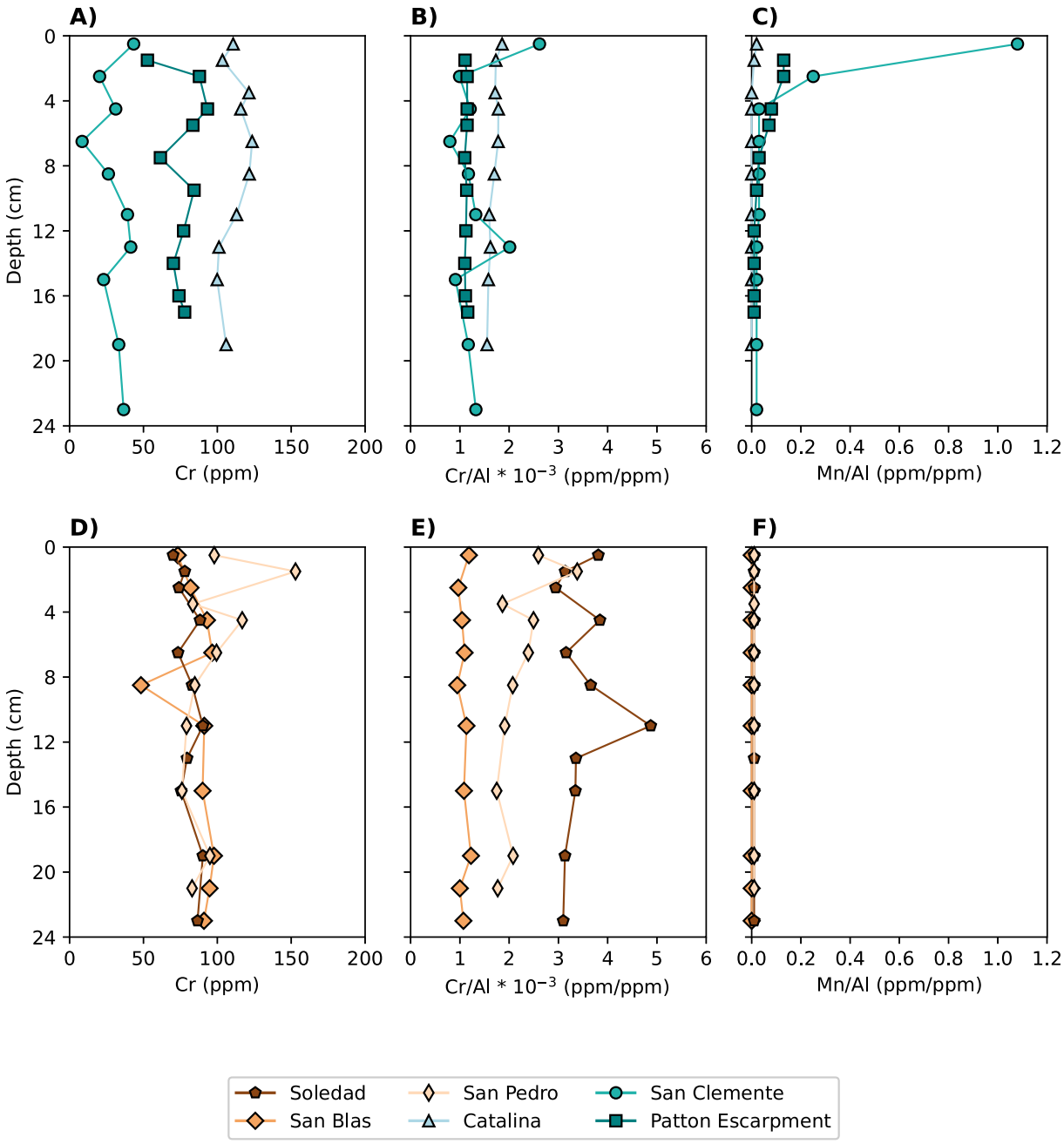

Fig. 5. Solid concentrations from sediment total digestions. The depth plots show concentrations of Cr, Cr/Al and Mn/Al in the sediment of more oxic and organic-poor stations (upper panel), and of organic-rich stations (lower panel).

the surface sediment, are low compared with the other sites ($\leq$13.5 nmol cm^{-2} y^{-1}; Table 6). At the Catalina Basin site, where bottom water oxygen concentrations are only 19 μM, Cr MAR is slightly higher (31.2 nmol cm^{-2} y^{-1}; Table 6). At this site, the surface sediment was not oxygenated (Chong et al., 2012). Dissolved Mn concentrations in pore fluids at this site do not increase with depth (Fig. 3), indicating that there is no Mn released from reductively dissolving Mn oxides. Thus, Mn oxides are not expected to be present.

Our data from the San Clemente Basin and Patton Escarpment sites show that below the oxygen penetration depth (horizontal blue dotted lines in Fig. 3), where Mn is released from the solid to the dissolved phase, we do not observe a distinct increase in dissolved Cr in pore fluids. This observation is in line with Shaw et al. (1990). We note that our newly collected data of Mn and Cr concentrations are in good agreement with previously published oxygen data, which were measured on samples collected $\geq$9 years before the samples studied here (Berelson et al., 1996; McManus et al., 2005; Chong et al., 2012). Pore fluid Cr concentrations were highest within the Mn enrichment zones at Patton Escarpment and San Clemente (Figs. 3 and 5). Note that Shaw et al. (1990) measured much higher Cr pore fluid concentrations (up to approximately 80 nM at Patton Escarpment), at least in part due to the much higher (mm scale) sampling resolution in their study. Below a sediment depth of 3.5 cm at the San Clemente site, dissolved Cr fluctuates but shows a trend towards slightly increasing Cr concentrations with depth (from 0.94 nM at 9.5 cm to 1.91 nM at 25.5 cm). At the same depth, dissolved Mn concentrations increase.

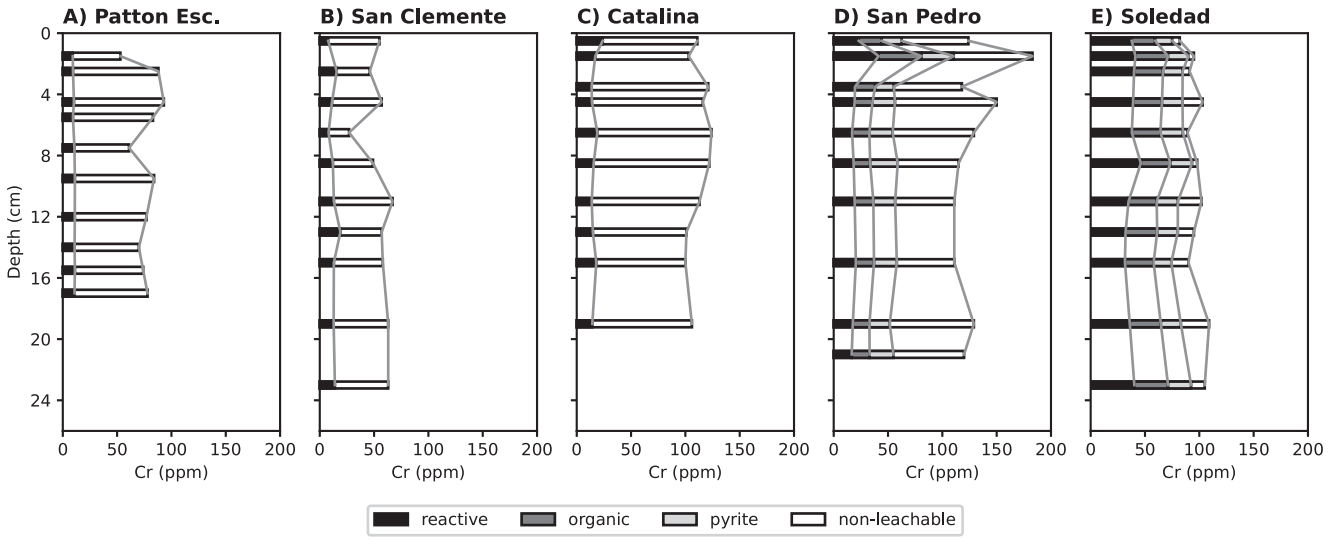

Fig. 6. Concentration data from sediment sequential extractions. The depth plots illustrate cumulative concentrations of Cr in sequential extractions of selected sediment samples. The non-leachable fraction is calculated as the difference between total Cr and Cr contained in the leached fractions.

This observation indicates that some Cr is released from the sediment to the pore fluids at the same depth where Mn is released. However, since the dissolved Cr increase is small and only occurs 9 cm below the increase in dissolved Mn, we argue that if any Cr is released from reductively dissolving Mn oxides, the proportion relative to the total Cr inventory is likely small. Indeed, previous studies found that Cr is not efficiently sorbed onto Mn oxides (Koschinsky & Hein, 2003; Neaman et al., 2004).

Dissolved Cr stays in solution, presumably as Cr(VI) (see Fig. 4 and discussion below), and can be transported via diffusion away from the zone where it was released. At the Patton Escarpment site, the pore fluid Cr maximum occurs below the sediment water interface, at 3 cm depth, leading to a gradient of dissolved Cr concentrations and hence, an estimated Cr benthic flux out of the sediment (-0.76 nmol cm^{-2} y^{-1}; Table 3). Also at the San Clemente site, the benthic Cr flux is directed out of the sediment (-0.43 nmol cm^{-2} y^{-1}; Table 3). However, at some oxic sites, the advective trace metal fluxes can be an order of magnitude higher than the diffusive fluxes (Lenstra et al., 2020). We therefore assume that our diffusive fluxes may underestimate total benthic fluxes. The idea that Cr is released into the pore fluids through oxidation – as suggested by Tang et al. (2014) – is confirmed by our speciation data, which show that virtually all dissolved Cr in pore fluids is present as Cr(VI) at the San Clemente basin, where Mn oxides are present (Fig. 4). Although we did not analyse speciation of Cr in the pore fluids from the Patton Escarpment site, Tang et al.'s experimental findings, coupled with our own observations at San Clemente, suggest that we would expect dissolved Cr(VI), rather than Cr(III), to be dominant at the Patton Escarpment site.

4.2. Chromium cycling under anoxic organic-rich conditions

Under organic-rich low-oxygen conditions in the water column at stations in proximity to our sampling sites (Fig. 1), dissolved seawater samples from the water column are depleted in Cr, whereas particulate matter is enriched in Cr and isotopically lighter (Murray et al., 1983; Huang et al., 2021). Further, seawater samples from the water column close to the sediment–water interface are enriched in Cr compared with shallower samples at a station close to the Soledad site (Murray et al., 1983). In pore fluids, Cr concentrations are tightly linked to the distribution of organic matter (Brumsack and Gieskes, 1983). These authors found increasing dissolved Cr concentrations with sediment depth, with concentrations typically below 100 nM. The high dissolved Cr concentrations at depth can be facilitated by the complexation of Cr with organic compounds (Brumsack and Gieskes, 1983). Shaw et al. (1990) note that increasing productivity, as well as very low bottom water oxygen levels, should promote the accumulation of Cr in the sediment. In addition to input of Cr with particulate matter, under anoxic conditions, Cr can accumulate in anoxic sediments via reduction by microorganisms or Fe(II) in the water column or in the sediment (e.g., Kitchen et al., 2012; Reinhard et al., 2014). In the Santa Barbara Basin (close to our oxic sites; Fig. 1), Fe(II) has been proposed as a potential reductant of Cr in both the anoxic bottom and pore waters (Moos et al., 2020).

The Cr MAR at the anoxic sites are typically higher than at the oxic sites ($\geq$31.7 nmol cm^{-2} y^{-1}; Table 6). In line with this observation, particulate matter in an oxygen minimum zone close to the Soledad station was enriched in Cr compared with the dissolved phase (Murray et al., 1983). These observations indicate that the transport of Cr from the water column to the sediment is enhanced in environments with high productivity and C_{org} burial rates. At the sites from this study with the highest C_{org} burial rates (Table 6) and the highest TOC contents (average of 7.2 wt% and 5.0 wt% for Soledad and San Blas, respectively; Fig. 2; Table 4), we observe the highest dissolved Cr concentrations in pore fluids, reaching up to 77 nM at approximately 20 cm depth (Fig. 3). At both sites, dissolved Cr concentrations show a steady increase with sediment depth until our deepest sample. These findings are in good agreement with the findings of Brumsack and Gieskes (1983) discussed earlier in this section. Further, our data confirm the possibility of Cr reduction by dissolved Fe in the pore fluids as proposed for the Santa Barbara Basin (Moos et al., 2020) as evidenced by the presence of dissolved Fe in the (surface) sediments (Fig. 3).

In the C_{org}-rich surface sediment, Cr is likely released into the pore fluids as the organic carbon carrier phase is remineralised during early diagenesis. The decrease of TOC between surface sediments and samples from $\approx$2–5 cm sediment depth shows evidence for the decomposition of organic matter (Fig. 2). These observations support the thesis that Cr cycling is tightly linked to C_{org} cycling (e.g., Janssen et al., 2021). At the San Pedro station, where sediment TOC content averages 4.3 wt%, the dissolved Cr concentrations in pore fluids also increase with depth. However, the dissolved Cr concentrations are considerably lower ($\approx$9 nM

Table 5
Concentration data from sediment sequential extractions.

Station	Depth cm		$Fe_{reactive}$ %	$Mn_{reactive}$ ppm	$Cr_{reactive}$ ppm	$Ni_{reactive}$ ppm	$Fe_{organic}$ ppm	$Cr_{organic}$ ppm	$Ni_{organic}$ ppm	$U_{organic}$ ppm	Cr_{pyrite} ppm	Ni_{pyrite} ppm	U_{pyrite} ppm
Patton Escarpment	1	2	0.54	5465	9.1	152.1							
	2	3	0.56	5981	9.4	160.2							
	4	5	0.58	4499	10.3	120.5							
	5	6	0.54	3465	9.3	102.6							
	7	8	0.53	1579	10.7	86.0							
	9	10	0.45	583	11.1	84.0							
	11	13	0.55	296	11.1	73.1							
	13	15	0.56	195	10.9	58.8							
	15	16	0.56	172	11.1	63.1							
	16	18	0.41	136	10.8	60.6							
San Clemente	0	1	0.36	25,802	7.7	67.3							
	2	3	0.47	10,787	15.6	89.6							
	4	5	0.62	1232	11.3	59.4							
	6	7	0.37	712	8.1	48.2							
	8	9	0.57	1122	12.1	74.8							
	10	12	0.41	572	13.0	70.6							
	12	14	0.66	981	19.0	100							
	14	16	0.44	624	13.0	69.0							
	18	20	0.41	624	12.8	68.2							
	22	24	0.42	696	13.9	66.5							
Catalina	0	1	0.76	581	23.9	38.3							
	1	2	0.88	123	17.1	28.4							
	3	4	0.45	54	13.7	27.7							
	4	5	0.42	48	14.0	29.3							
	6	7	0.39	48	19.0	38.2							
	8	9	0.42	56	15.6	31.8							
	10	12	0.39	47	13.8	28.9							
	12	14	0.41	51	14.8	30.8							
	14	16	0.38	56	18.0	37.6							
	18	20	0.38	55	14.3	30.6							
San Pedro	0	1	1.06	29	23.0	16.1	1910	20.9	9.9	0.33	18.6	11.2	0.08
	1	2	0.49	32	41.4	22.1	2036	39.4	11.6	0.57	29.7	14.1	0.12
	3	4	0.64	40	19.6	20.6	2225	18.6	11.4	0.59	17.1	11.1	0.10
	4	5	0.63	32	19.3	20.7	2488	16.4	10.7	0.43	20.7	13.4	0.09
	6	7	0.62	31	16.9	21.1	2487	15.9	10.4	0.39	21.5	13.3	0.09
	8	9	0.53	31	18.4	24.0	2211	15.2	10.1	0.44	25.4	15.0	0.10
	10	12	0.62	41	19.3	25.6	2077	17.2	10.7	0.44	20.0	12.4	0.08
	14	16	0.54	38	20.4	27.5	2079	16.7	10.1	0.49	21.0	12.7	0.08
	18	20	0.57	37	17.6	23.1	2183	15.3	9.3	0.47	18.7	11.7	0.09
	20	22	0.54	35	16.6	22.6	1973	16.5	9.9	0.47	21.9	13.3	0.09
Soledad	0	1	0.24	<LOD	37.8	26.6	994	21.5	9.17	0.82	15.8	8.57	0.07
	1	2	0.2	<LOD	41.2	29.1	790	30.0	10.5	1.13	18.7	9.2	0.10
	2	3	0.22	<LOD	40.0	26.6	985	26.6	10.7	1.26	18.1	9.1	0.09
	4	5	na	<LOD	39.0	25.2	878	26.6	11.0	1.29	18.9	9.7	0.10
	6	7	0.45	28	37.9	24.5	833	26.3	11.1	1.28	20.7	10.3	0.12
	8	9	0.22	1	46.2	31.0	1031	27.3	11.6	1.14	19.9	10.1	0.10
	10	12	0.24	1	34.9	24.5	1049	25.9	10.3	0.98	19.5	9.7	0.10
	12	14	0.18		32.1	21.9	1131	29.1	11.4	1.23	19.0	9.8	0.09
	14	16	0.2	<LOD	31.5	23.4	1019	26.4	10.8	1.14	16.3	8.6	0.08
	18	20	0.22	<LOD	36.0	25.9	972	28.6	10.9	1.11	18.4	9.2	0.10
	22	24	0.23	3	40.2	26.8	793	31.0	12.0	1.38	21.2	11.0	0.10

Elemental concentrations of the sequential extractions are shown. Please note that the H_2SO_4- and HNO_3-leaching steps were only conducted on samples from the Soledad and San Pedro sites.

Table 6
Chromium burial efficiency.

Station	Cr[a] ppm	Cr MAR[b] nmol cm^{-2} y^{-1}	Cr rain rate[c] nmol cm^{-2} y^{-1}	Cr burial efficiency[d]
Patton Escarpment	75.8	4.4	5.1	0.85
San Clemente	46.9	13.5	14.0	0.97
Catalina	116.1	31.3	31.2	1.00
San Pedro	136.6	76.2	76.3	1.00
San Blas	78.6	31.7	33.4	0.95
Soledad	92.8	89.3	92.9	0.96

The MAR, rain rates and burial efficiency of Cr was calculated for each station.
[a] Average Cr concentration of the upper 10 cm of the sediment.
[b] Calculated as the product of MAR and Cr concentration.
[c] Calculated as the sum of the negative Cr benthic flux and MAR.
[d] Calculated as the Cr MAR divided by the Cr rain rate.

maximum) at the San Pedro site compared to the more anoxic sites. This shift to lower Cr concentrations is partly in line with the lower C_{org} content of the sediment, thereby releasing less Cr during diagenesis as compared to stations with higher C_{org} burial rates and higher C_{org} content (Soledad and San Blas). However, we note that pore fluid Cr concentrations in San Pedro are up to 3 times higher than at the Catalina site, despite similar TOC contents (average 4.8 wt%).

Our Cr speciation data in Fig. 4 show that at the oxygen-poor, C_{org}-rich sites (Soledad, San Blas and San Pedro), between approximately 40 and 80% of the total dissolved Cr in pore fluids is Cr(III) (Table 2). This proportion of Cr(III) is much higher compared with the Mn-rich site with lower C_{org} at San Clemente, where all dissolved Cr is present as Cr(VI). This higher abundance of dissolved Cr(III) is consistent with observations from the water column of prominent oxygen minimum zones or restricted anoxic basins (e.g., Emerson et al., 1979; Rue et al. 1997; Davidson et al., 2019; Huang et al., 2021). These authors observe that under reducing marine conditions, Cr(III) can be the dominant dissolved Cr species. Thus, we propose that Cr(III) can be preferentially released to the pore fluid under anoxic conditions during diagenesis. This observation sharply contrasts the calculations of Moos et al. (2020), who proposed that dissolved Cr concentrations would be exhausted at a sediment depth of <1 mm.

Further, Cr(III) is thought to be the main Cr species sorbing onto organic matter (Semeniuk et al., 2016) and it is therefore more tightly linked to organic matter compared with Cr(VI). This behaviour likely leads to the observed pattern of Cr speciation under anoxic C_{org}-rich and oxic conditions. Anoxic bottom water at Soledad and San Blas further allow for any adsorbed Cr(III) that might be scavenged within the water column to remain particle-bound after its transition from the water column to the sediment.

As at the more oxic sites, the estimated benthic fluxes (see Section 2.6) of Cr are directed out of the sediment at all C_{org}-rich sites (Table 3), indicating that some proportion of Cr is cycling back into the bottom water. Any biologically driven advective fluxes at these sites are likely minor due to the anoxic bottom water conditions. The largest estimated benthic flux is found at the Soledad site (-1.91 nmol cm^{-2} y^{-1} when using the diffusion coefficient of Cr (III) rather than Cr(VI; Table 3) coinciding with the highest TOC content (maximum of 8.2 wt%). Despite the estimated uncertainty, the fluxes at the C_{org}-rich sites would still be larger than those at the oxic stations. The observation that the largest estimated benthic flux co-occurs with the highest TOC content indicates that Cr is released from sediments with high TOC contents and thus, organic matter can be a major carrier of Cr (see also Section 4.3.1). Still, the benthic flux at the Soledad site is on the same order of magnitude as the one determined for a carbonate-rich (76%) sediment core from the Tasman Sea, comprising only 1% of organic matter (-3 nmol cm^{-2} y^{-1}; Janssen et al., 2021). Despite the similar estimated benthic Cr flux, dissolved Cr in pore fluids shows an inverse trend in the carbonate-rich sediment from the Tasman Sea compared with our C_{org}-rich sites, decreasing with sediment depth. Thus, while leading to a similar benthic flux of Cr, the processes driving the dissolved Cr distribution within these contrasting sites are likely different. At the Soledad and San Blas sites, we do not observe a decrease in total dissolved Cr concentrations within the upper 20 cm, unlike for our sites where a Mn oxide-rich layer borders the sediment–water interface. However, the Cr speciation data from Soledad show a slight decrease of dissolved Cr(VI) concentrations below 15 cm sediment depth (Fig. 4). This decrease can be the result of reduction of Cr(VI) to Cr(III), leading to an increase in dissolved Cr(III). Overall, it seems that under the anoxic conditions prevailing at the Soledad and San Blas sites, at least 46% of total Cr is present as Cr(III) in the pore fluids (and a maximum of 79%).

4.3. Chromium preservation in sediments

4.3.1. Assessment of the sequential extraction procedure

We assess the sequential extraction procedure applied in this study in the context of the oxic C_{org}-poor Mn-rich, and the anoxic C_{org}-rich sediment samples. Our data from sequential extractions indicate that Cr associated with organic matter is contained in both the reactive and the organic sediment fractions with correlation coefficients of $\geq$0.71 (Fig. 7). In sediments deposited under oxic conditions, where Mn (and Fe) oxides occur, the first leaching step (1 M HCl) is thought to efficiently release metals associated with Mn and Fe (oxyhydr)oxides, and other sediment fractions that easily dissolve (e.g., carbonates, phosphate minerals, hydrous aluminosilicates and Fe monosulfides; Huerta-Diaz and Morse, 1990; Scholz et al., 2014). In addition, metals can be released from clay or biogenic particles (Bruggmann et al., 2019; Frank et al., 2020). Two of the stations investigated here (Patton Escarpment and San Clemente) contain high Mn concentrations (10,000 ppm and higher) and Mn oxides. Due to the important role of Mn oxides as catalysts for Cr oxidation (van der Weijden and Reith, 1982; Manceau et al., 1992), we focus on the potential association of Cr with Mn, rather than with Fe, even though the reactive fraction comprises metals associated with both, Mn and Fe (oxyhydr)oxides. Our data show that the reactive fraction contains typically between 50 and 100% of the total Mn. In addition, Ni – an element that sorbs onto Mn oxides (e.g., Koschinsky and Hein, 2003) and is also linked to biological cycling (e.g., Böning et al., 2015) – shows a strong correlation with Mn in the reactive fraction (R^2 = 0.79; Fig. S1), indicating that this leaching step successfully dissolved Mn oxides. Neither $Mn_{reactive}$ nor $Fe_{reactive}$ show a positive correlation with $Cr_{reactive}$ (Fig. S1). This observation provides an indication that Cr is not predominantly associated with Mn and Fe oxides, and that the distribution of Cr is dominated by other phases. The concentrations of Ti in the reactive fraction, which can be used to assess detrital contribution, were all below the limit of detection (0.003 ppm). Thus, as previously observed for 0.5 M HCl, the detrital fraction is not appreciably attacked in this leaching step (Frank et al., 2020). This notion is in agreement with the findings by Frank et al. (2020) who found low Ti, as well as Al, concentrations in sediment fractions leached with 0.5 M HCl. Frank et al. (2020) show that even 6 M HCl leaches typically less than approximately 20% of total Al, and <10% of total Ti. Thus, even though our leaching procedure used 1 M HCl rather than 0.5 M HCl, we estimate an upper limit of <20% of Cr contribution from the detrital fraction.

The proportions of Cr extracted in each leaching step likely differ in sediments deposited under anoxic conditions with high TOC content compared with oxic C_{org}-poor sediments with Mn oxides. While the reactive fraction comprises trace metals associated with easily-dissolvable fractions such as Fe and Mn(oxyhydr)oxides or with clays, the contribution of trace metals that are associated with biogenic particles is likely larger in samples with high TOC compared with TOC-poor samples (Bruggmann et al., 2019; Frank et al., 2020). We find positive correlations between Cr concentrations in the organic as well as reactive fractions with C_{org} (R^2 = 0.71 and R^2 = 0.95, respectively; Fig. 7). These correlations further support the notion of a link between Cr and organic matter, which can be associated with both the organic and reactive fractions. In addition, Ti concentrations in the reactive fractions of the organic-rich sites were below detection limit (0.003 ppm).

Based on our data, we propose that Cr(III) sorbed onto the surface of organic matter is found in the reactive fraction, whereas Cr incorporated into organic matter is in the organic fraction. The Cr concentrations in the reactive fraction are higher compared with the ones in the organic fraction. Under the simplified assumptions that at the Soledad and San Pedro sites, all Cr associated with organic matter is contained within the organic and reactive frac-

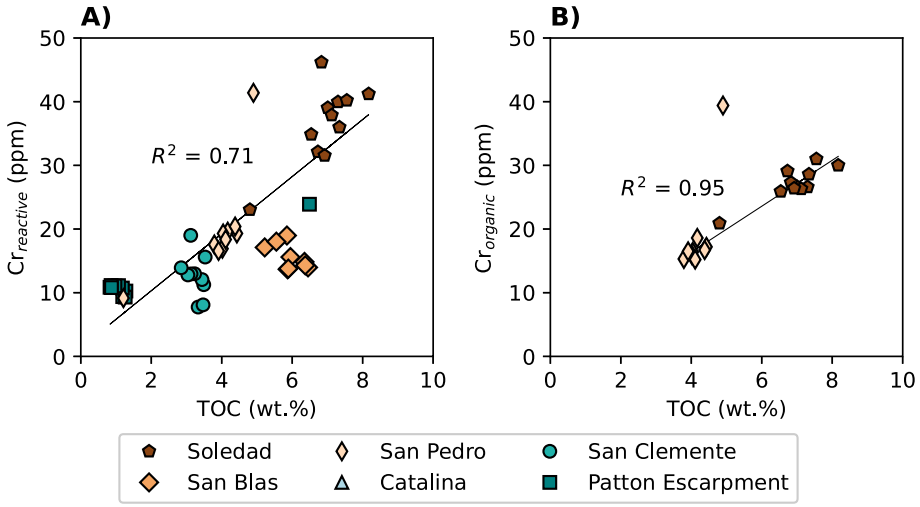

Fig. 7. Link between Cr and organic matter. The cross-plots show sedimentary Cr in (A) $Cr_{reactive}$ and (B) $Cr_{organic}$ versus TOC contents. In (B), R^2 does not include the outlier.

tions, and that all Cr in these fractions is exclusively associated with organic matter, up to 64% of Cr associated with organic matter is surface-bound in some samples, whereas other samples have a maximum of 50% of total Cr is incorporated into organic matter. If we assume that 20% of Cr in the reactive fractions is contributed by the detrital fraction, up to 58% of organic-associated Cr could be surface-bound. Regardless of the detrital contribution, these proportions are consistent with those reported in Semeniuk et al. (2016), who found that between 26 and 67% of total Cr associated with phytoplankton cells can be extracellular.

The organic fraction, which is contained in the leaching step using H_2SO_4, shows a strong positive correlation between the bioactive elements $Ni_{organic}$ and $U_{organic}$ (R^2 = 0.72; Fig. S2) at the Soledad station. Since both of these elements are bioactive, this correlation suggests that this leaching fraction likely contains elements that are associated with organic matter. Chromium contained in the organic fraction is moderately well correlated with $Ni_{organic}$ and $U_{organic}$, (R^2 = 0.59 for $Ni_{organic}$ and $Cr_{organic}$ and R^2 = 0.47 for $U_{organic}$ and $Cr_{organic}$ at the Soledad site; Fig. S2) and supporting the idea that organic matter is a source of Cr. Furthermore, the $Cr_{organic}$ and TOC show a positive correlation (R^2 = 0.95 if one outlier is excluded; Fig. 7), providing an additional line of evidence for the association of Cr with organic matter.

The elemental concentrations comprised within the leaching fraction containing pyrite (leached using HNO_3) show a strong positive correlation between Ni_{pyrite} and Cr_{pyrite} at the Soledad and the San Pedro sites (R^2 = 0.90 or 0.70; Fig. S3). At the former station, the decrease of dissolved Fe concentrations in pore fluids co-occurring with the increase in H_2S (Figs. 2 and 3) indicates precipitation of pyrite. Since Ni is readily scavenged by pyrite (e.g., Morse and Luther, 1999), the positive correlation between Ni_{pyrite} and Cr_{pyrite} can indicate that at this site, Cr is contained in the pyrite fraction. Interestingly, approximately 18% of sediment Cr is associated with the pyrite fraction. This finding is surprising since Cr is not thought to be associated with pyrite (e.g., Morse and Luther, 1999). We speculate that Cr that is released from decomposing organic matter may be sorbed onto Fe sulfide minerals, perhaps transiently. However, since Cr was previously not found to be incorporated into pyrite, this interpretation is notably speculative. Perhaps more convincingly, we note that if the H_2SO_4-leaching step did not quantitatively extract the organic fraction, residual organics would dissolve in the HNO_3-leaching step. Detailed assessment of the potential relationship between Cr and pyrite would exceed the scope of this study. The leaching protocol used here may simply prevent admixture of pyrite-associated metals with the organic sediment fraction, since it is using H_2SO_4 to dissolve trace metals associated with organic matter and not with pyrite, as opposed to HNO_3, which would contain metals from both organic matter and pyrite unless the organics are previously removed (e.g., Huerta-Diaz and Morse, 1992).

4.3.2. Insights from oxic organic-poor sediments

We use the solid-phase geochemical data to assess the transfer of Cr from pore fluids to sediments. In line with the dissolved Cr data, the oxic C_{org}-poor sites all have low Cr concentrations as well as low Cr/Al ratios (Figs. 3 and 5). At the same sediment depth where we observe oxidative release of Cr(VI), Cr/Al in San Clemente is slightly elevated ($2.6 * 10^{-3}$ ppm/ppm; Fig. 5). This peak is likely the result of low Al in the surface sediment sample (approximately 21,000 ppm, compared with typically >40,000 ppm in the deeper samples; Table 4), rather than being related to the elevated Cr, but is noted here for completeness. The low Al concentration in this sample might be due to the abundance of Mn oxides, which is evidenced by the high Mn concentration, and smaller contribution of detrital material to the sediment compared to other samples from this core. At greater sediment depth, Cr to Al ratios at the San Clemente site remain relatively constant, similar to the values observed at the Patton Escarpment site (approximately $1.1 * 10^{-3}$ ppm/ppm; Fig. 5B). Even though dissolved Cr in pore fluids is enriched in the oxidised zone, where Mn occurs in a solid phase, we do not observe solid-Cr peaks co-occurring with solid-Mn peaks. Thus, dissolved Cr is not appreciably accumulated in the solid phase in sediments at stations with Mn oxides. Instead, this Cr is readily released from the sediment to the bottom water.

The sequential extraction data provide additional evidence that solid-phase Cr is not associated with solid-phase Mn, as previously suggested by Shaw et al. (1990; Fig. 6). The reactive fraction does not show an enrichment of Cr in the surface sediment, where Mn oxides are present (Fig. 6; Table 5). The outcome of Cr release from the sediment under conditions with a sediment Mn-rich zone is that there is no Cr enrichment in the sediment. Instead, as Cr passes through a Mn-rich zone during burial, it leaves behind a Cr-poor sediment package. Oxidative loss of Cr in the presence of Mn oxides can lead to a small benthic flux directed out of the sediment (between −0.76 and −0.43 nmol cm^{-2} y^{-1}; Table 3). As noted earlier, these benthic Cr fluxes are smaller than those published for a station in the Tasman Sea with oxic conditions (−3 nmol cm^{-2} y^{-1}; Janssen et al., 2021). In combination, the

benthic fluxes of Cr calculated in this study for all sites (−1.91 to + 0.03 nmol cm^{-2} y^{-1}) span a range that is consistent with previous estimates (−3 to −0.1 nmol cm^{-2} y^{-1}; Janssen et al., 2021; Pöppelmeier et al., 2021). We note that at the stations investigated here and the one investigated by Janssen et al. (2021), a benthic flux from sediment to water column is a common feature at all sites. This observation is noteworthy since the stations span a large range of environmental and redox conditions, and the size of local Cr benthic fluxes seems to vary substantially. Data from further sites as well as studies that specifically target the identification of *in situ* benthic fluxes are required to quantify a representative global benthic flux of Cr.

Estimated benthic fluxes, in combination with the Cr burial rate, allow us to examine the estimated Cr burial efficiency, which provides further insights into the preservation of Cr in the sediment record. We use the estimate of the burial efficiency of total sediment Cr, rather than of authigenic Cr, due to uncertainties in the estimate of detrital Cr/Al ratios. Regardless of the use of bulk or authigenic Cr concentrations for burial efficiency calculations, the resulting burial efficiencies are similar to each other (Table S2). This observation highlights that due to the high burial efficiency, interpretations of bulk sediment Cr are not biased by changes in detrital matter. Even though Cr burial is quite efficient at all sites studied here, the site where the sediment underlies the most oxic water column, Patton Escarpment, is the site where we observe the lowest burial efficiency (0.85; Table 6). Our pore fluid concentration data show that this relatively lower Cr burial efficiency is likely the result of oxidative loss of Cr (see Section 4.1). Despite the results from Patton Escarpment, the overwhelming pattern under largely oxidising conditions is that much of the Cr that arrives at the seafloor is buried (estimated burial efficiencies of ≥0.85).

4.3.3. Insights from anoxic organic-rich sediments

At the station with the highest TOC content (Soledad; Figs. 5 and 6), we observe the highest Cr concentrations in sediments (Cr/Al and Cr in reactive fraction). This observation again supports the thesis that Cr accumulation is tightly linked to organic matter. Sediments with higher organic matter content have higher Cr concentrations, which are retained in the sediment under anoxic conditions. The San Blas site falls off the trend between Cr in the organic fraction and TOC, shifting towards lower Cr concentrations. This finding confirms our observation that at the San Blas site, lithogenic Cr input seems to have a stronger impact on the solid phase Cr distribution in the sediment compared with the other sites (Supplementary Material). The Cr:C ratios of sediments from Soledad and San Blas range between 191 and 394 μmol/mol (Table 5). These ratios are close to the upper limit of Cr:C ratios found in phytoplankton-dominated particulate matter from the Celtic Sea (10–297 μmol/mol; Dauby et al., 1994; Semeniuk et al., 2016). It is thus possible that organic matter is indeed a major source of Cr in the sediments from the Soledad and San Blas sites, however, we note that the typical Cr:C ratios for the Celtic Sea (mean of 65 μmol/mol; Dauby et al., 1994) and the Cariaco basin (10–40 μmol/mol; Calvert et al., 1991) are lower than the Cr:C ratios measured in the sediments studied here. However, the Cr:C ratios used here include not only authigenic but also detrital Cr and are therefore overestimating the Cr:C. Additional data of Cr:C in biogenic particles are required to confirm if Cr is mainly sourced from biogenic particles at the Soledad and San Blas sites.

The sequential extractions seem to contain Cr associated with organic matter in both the reactive and organic sediment fractions (see Section 4.3.1). The lack of variation of Cr in the organic and reactive fractions with depth indicates that Cr associated with organic matter is preserved in the sediment (Fig. 7). Under the assumption that the reactive and organic fractions contain both sorbed and structurally incorporated Cr, respectively (Section 4.3.1), we hypothesise that Cr associated with organic matter is well preserved in the sediment, regardless of its association with organic matter.

The Soledad and San Pedro sites have higher Cr burial efficiencies than the San Blas site (Table 6), indicating that at the former two sites, nearly all Cr that is delivered to the seafloor is buried within the sediment. The MAR at San Blas is lower compared with Soledad (21 and 50 mg cm^{-2} y^{-1}, respectively; Table 1; McManus et al., 2006a, 2006b; Poulson et al., 2006). The estimated Cr benthic flux at San Blas is also lower than at Soledad (Table 3), and thus, the estimated burial efficiency of Cr is nearly identical at these two sites (≈0.95; Table 6). For the San Pedro site, we calculate a burial efficiency of 1 (Table 6). Interestingly, although the estimated benthic Cr fluxes are largest at the anoxic sites (up to −1.91 nmol cm^{-2} y^{-1}), the Cr burial efficiency is not reduced significantly. The lack of a reduced Cr burial efficiency is because the dissolved benthic flux out of the sediment is relatively small compared to the very efficient delivery of Cr by (biogenic) particles, either as sorbed or incorporated Cr. Despite the uncertainties accompanying our benthic flux and burial efficiency estimates, the high C_{org} burial rate, in combination with the positive correlation of sedimentary Cr and TOC, support the notion that Cr accumulates in C_{org}-rich sediments. Consequently, a large proportion of Cr that reaches the sediment at these sites is buried with the sediment record, despite the presence of an estimated Cr benthic flux directed out of the sediment that is up to ≈8 times larger than at oxic sites.

5. Implications for the Cr isotope system as a paleoproxy

Our data show strong dependencies of Cr on both redox conditions and biological processes, which can create characteristic patterns in the distribution of Cr in surface sediments and pore fluids. However, these characteristic patterns can undergo modification during early diagenesis, which potentially alters the Cr isotope compositions recorded by the sediment. Based on our concentration data, we seek to link the pathway of Cr from the water column to the sediment, and speculate on how Cr isotope compositions could be affected at the sediment–water interface.

The Cr MAR provides an indication of transport of Cr from the water column to the sediment. At the anoxic sites, where C_{org} burial rates are high, typically also the Cr MAR and the Cr rain rates are higher when compared with the oxic sites (both ≥31.7 nmol cm^{-2} y^{-1}; Table 6). It is noteworthy that the Cr rain rates calculated here span a smaller range (5–93 nmol cm^{-2} y^{-1}; Table 6) compared with Cr output fluxes used for global Cr budgets (up to one order of magnitude higher than our Cr rain rates; e.g., Reinhard et al., 2013; Wei et al., 2020). Pending future studies on Cr transport from the water column to the sediment, these global Cr budgets may need to be reassessed.

Based on our data, it seems likely that in highly productive environments, where C_{org} is well preserved in the sediment, Cr accumulation along with sinking organic matter is enhanced. Chromium that is scavenged by particulate matter was proposed to be isotopically lighter than residual dissolved Cr by a fractionation factor of approximately 2‰ (Moos et al., 2020; Huang et al., 2021). However, sediments deposited under anoxic conditions in organic-rich sediments on the Peruvian margin were found to have higher Cr isotope compositions compared to samples deposited under oxic conditions (Bruggmann et al., 2019). Our data indicate that Cr accumulation in organic-rich sediments is at least in part sourced from the water column, providing support for previous findings (Murray et al., 1983; Huang et al., 2021). Alternatively, Cr reduction at the sediment–water interface can be enhanced in sediments depositing under anoxic conditions, leading to Cr

accumulation with Cr sourced from the bottom water. However, our benthic flux estimates for most stations indicate a flux out of the sediment, rather than a flux into the sediment (Table 3). In addition, under the assumption that our leaching protocol effectively isolated organic-bound Cr, a considerable proportion of Cr is contributed by the organic fraction. Therefore, abiotic accumulation of bottom-water-sourced Cr under anoxic C_{org}-rich conditions is unlikely the dominant pathway of Cr to the sediment. Further, the positive correlation of reactive Cr and TOC is observed under both anoxic and oxic conditions. This finding is in line with data from the Peruvian margin, where a positive correlation between excess Cr and TOC was observed across sites with oxic to anoxic conditions (Bruggmann et al., 2019). Since Cr reduction and accumulation across the sediment–water interface is not favoured under oxic bottom water conditions, these observations provide support for the importance of water-column-sourced Cr accumulation with organic matter, under both anoxic and oxic conditions.

For oxic sites, we observe that the Cr delivery to the sediments and the estimated Cr burial efficiency are lower, the latter due the oxidative loss of dissolved Cr from pore fluids to the bottom water. Coupled with redox transformations of Cr – which typically produces a relatively large Cr isotope fractionation (e.g., Ellis et al., 2002a, 2002b; Zink et al., 2010; Miletto et al., 2021) – we speculate that the isotope composition of authigenic Cr in oxic sediments is likely to undergo modification during burial. Isotope fractionation might lead to enrichment of isotopically light Cr in Fe-Mn rich sediments, as suggested by Wei et al. (2018). At the anoxic C_{org}-rich sites, in contrast, loss of Cr from the sediment via a benthic flux is dwarfed by the high rate of Cr delivery to the sediments in association with biogenic particles. Thus, Cr efflux from the sediment under reducing conditions might not induce significant Cr isotope fractionation. However, we speculate that due to the significant contribution of water-column-sourced Cr, which is expected to be isotopically lighter than seawater (Moos et al., 2020; Huang et al., 2021), the sediment might be isotopically lighter than the overlying water column. This interpretation follows a recent study that found non-quantitative Cr removal under anoxic conditions, leading to an isotopic offset of these sediments from the water column (Janssen et al., 2022). Due to the high burial efficiency of Cr, we hypothesise further that the authigenic isotope composition of Cr that reaches the sediment may be reasonably well preserved in the sediments underlying ocean regions with high surface biological productivity. Thus, our study indicates that while early diagenetic reactions may have the potential to alter the Cr isotope composition in the sediments, these reactions occur in direct response to the local depositional conditions, producing authigenic Cr enrichments and potentially a Cr isotope signature that may reflect – with perhaps an isotopic offset – a combination of surface productivity as well as redox conditions. Since our data set does not include Cr isotope analyses, these hypotheses need to be confirmed in future studies.

6. Conclusions

Chromium and its isotopes have the potential to serve as a powerful proxy to reconstruct redox conditions as well as biological productivity. The utility of this proxy, however, is limited by our understanding of Cr cycling in modern marine environments. We provide insights into Cr pathways from bottom water to and burial within the sediment, contributing to our understanding of how Cr is preserved in the sedimentary record under a range of relevant redox and C_{org} burial conditions.

Our study supports previous findings by Shaw et al. (1990), that under C_{org}-poor oxic conditions with high solid Mn concentrations near the sediment–water interface, a portion of the Cr(III) undergoes oxidation to Cr(VI) by Mn oxides. The oxidised Cr(VI) stays in solution as evidenced by our speciation data, and is effluxed to the bottom water. The site where the sediment underlies the most oxic water column shows the lowest Cr burial efficiency. Under anoxic C_{org}-rich conditions, Cr is released from decomposing organic matter within the sediment, and is kept in solution likely due to complexation of Cr(III) with organic compounds. Consequently, dissolved Cr concentrations in pore fluids show a steady increase with sediment depth as previously suggested by Brumsack and Gieskes (1983).

The considerable contribution of the organic fraction to total Cr, and the strong positive correlation between TOC and Cr in the organic and reactive fractions at all sites provide evidence of the close link between Cr and organic matter. Thus, shuttling of Cr with organic matter from the water column to the sediment is likely an important pathway of Cr to both anoxic and oxic sediments. Therefore, a significant amount of Cr in the sediment record may not be directly associated with redox changes. Even though the estimated benthic Cr fluxes directed out of the sediment at the anoxic sites are larger than at the oxic sites, the estimated Cr burial efficiency is not significantly reduced. Virtually all Cr that reaches the sediment is buried in the sediment record.

Declaration of Competing Interest

The authors declare that they have no known competing financial interests or personal relationships that could have appeared to influence the work reported in this paper.

Acknowledgements

We thank crew members and the researchers for their efforts and time in collecting sample material at sea. We would also like to thank Katie Squires, Sara Rauschenberg, Miguel Angel Huerta-Diaz, Dominique Iaccarino and William Biggs for their support in sample collection, preparation, and analysis. We thank the editor Noah Planavsky as well as David Janssen and two anonymous reviewers for their constructive comments that helped to improve the initial version of the manuscript. This research was supported by NSF [grants OC-1657832 to J. McManus and OC-1657690 to S. Severmann).

Appendix A. Supplementary material

The Supplementary Material contains detailed information on the contribution of authigenic Cr (Section 1) to the total Cr, as well as an assessment of Al concentrations at the San Blas station (Section 2). Further, the contribution of authigenic Cr to the Cr burial efficiency is estimated (Section 3). In addition, cross-plots of a range of concentrations in solid and dissolved samples are presented in support of our discussion in the main text. Supplementary material to this article can be found online at https://doi.org/10.1016/j.gca.2023.03.003.

References

Banerjee, D., Nesbitt, H.W., 1999. Oxidation of aqueous Cr (III) at birnessite surfaces: Constraints on reaction mechanism. Geochim. Cosmochim. Acta 63, 1671–1687.
Bartlett, R., James, B., 1979. Behavior of Chromium in Soils: III. Oxidation. *J. Environ. Qual.* 8, 31–35.
Basu, A., Johnson, T.M., Sanford, R.A., 2014. Cr isotope fractionation factors for Cr(VI) reduction by a metabolically diverse group of bacteria. Geochim. Cosmochim. Acta 142, 349–361.
Bauer, K.W., Gueguen, B., Cole, D.B., Francois, R., Kallmeyer, J., Planavsky, N., Crowe, S.A., 2018. Chromium isotope fractionation in ferruginous sediments. Geochim. Cosmochim. Acta 223, 198–215.

Berelson, W.M., Hammond, D.E., Johnson, K.S., 1987. Benthic fluxes and the cycling of biogenic silica and carbon in two southern California borderland basins, United States. *Geochim. Cosmochim. Acta* 51, 1345–1363.
Berelson, W.M., McManus, J., Coale, K.H., Johnson, K.S., Kilgore, T., Burdige, D., Pilskaln, C., 1996. Biogenic matter diagenesis on the sea floor: A comparison between two continental margin transects. J. Mar. Res. 54, 731–762.
Böning, P., Shaw, T., Pahnke, K., Brumsack, H.J., 2015. Nickel as indicator of fresh organic matter in upwelling sediments. Geochim. Cosmochim. Acta 162, 99–108.
Boudreau, B.P., 1996. Diagenetic Models and Their Implementation. Springer, Heidelberg.
Bruggmann, S., Scholz, F., Klaebe, R.M., Canfield, D.E., Frei, R., 2019. Chromium isotope cycling in the water column and sediments of the Peruvian continental margin. Geochim. Cosmochim. Acta 257, 224–242.
Brumsack, H.J., Gieskes, J.M., 1983. Interstitial water trace-metal chemistry of laminated sediments from the Gulf of California, Mexico. *Mar. Chem.* 14 (1).
Calvert, S., Karlin, R., Toolin, L., Donahue, D.J., Southon, J.R., Vogel, J.S., 1991. Low organic carbon accumulation rates in Black Sea sediments. Nature 350, 692–695.
Campbell, J.A., Yeats, P.A., 1984. Dissolved chromium in the St. Lawrence estuary. *Estuar. Coast. Shelf Sci.* 19, 513–522.
Canfield, D.E., 1988. Sulfate Reduction and the Diagenesis of Iron in Anoxic Marine Sediments. Yale University.
Chong, L.S., Prokopenko, M.G., Berelson, W.M., Townsend-Small, A., McManus, J., 2012. Nitrogen cycling within suboxic and anoxic sediments from the continental margin of Western North America. Mar. Chem. 128–129, 13–25.
Cole, D.B., Zhang, S., Planavsky, N.J., 2017. A new estimate of detrital redox-sensitive metal concentrations and variability in fluxes to marine sediments. Geochim. Cosmochim. Acta 215, 337–353.
Cranston, R.E., Murray, J.W., 1978. The determination of dissolved chromium species in natural waters. Anal. Chim. Acta 99, 275–282.
Dauby, P., Frankignoulle, M., Gobert, S., Bouquegneau, J.-M., 1994. **Distribution of poc, pon, and particulate al, cd, cr, cu, pb, ti, zn and delta-c-13 in the english-channel and adjacent areas**. Oceanologica Acta 17 (6), 643–657.
Davidson, A.B., Semeniuk, D.M., Koh, J., Holmden, C., Jaccard, S.L., Francois, R., Crowe, S.A., 2019. A $Mg(OH)_2$ coprecipitation method for determining chromium speciation and isotopic composition in seawater. Limnol. Oceanogr. Methods.
Døssing, L.N., Dideriksen, K., Stipp, S.L.S., Frei, R., 2011. Reduction of hexavalent chromium by ferrous iron: A process of chromium isotope fractionation and its relevance to natural environments. Chem. Geol., 157–166.
Eary, L.E., Rai, D., 1987. Kinetics of Chromium (III) Oxidation to Chromium (VI) by Reaction with Manganese Dioxide. Environ. Sci. Technol. 21, 1187–1193.
Elderfield, H., 1970. Chromium speciation in sea water. Earth Planet. Sci. Lett. 9, 10–16.
Ellis, A.S., Johnson, T.M., Bullen, T.D., 2002a. Chromium isotopes and the fate of hexavalent chromium in the environment. Science 295, 2060–2062.
Ellis, A.S., Johnson, T.M., Bullen, T.D., 2002b. Chromium isotopes and the fate of hexavalent chromium in the environment. Science 295 (5562), 2060–2062.
Emerson, S., Cranston, R.E., Liss, P.S., 1979. Redox species in a reducing fjord: Equilibrium and kinetic considerations. Deep Sea Res. Part A Oceanograph. Res. Pap. 26, 859–878.
Fendorf, S.E., 1995. Surface reactions of chromium in soils and waters. Geoderma 67, 55–71.
Fendorf, S.E., Fendorf, M., Sparks, D.L., Gronsky, R., 1992. Inhibitory Mechanisms of Cr(lll) Oxidation by ∂-MnO_2. J. Colloid Interface Sci. 153, 37–54.
Frank, A.B., Klaebe, R.M., Löhr, S., Xu, L., Frei, R., 2020. Chromium isotope composition of organic-rich marine sediments and their mineral phases and implications for using black shales as a paleoredox archive. Geochim. Cosmochim. Acta 270, 338–359.
Froelich, P.N., Klinkhammer, G.P., Bender, M.L., Luedtke, N.A., Heath, G.R., Cullen, D., Dauphin, P., Hammond, D., Hartman, B., Maynard, V., 1979. Early oxidation of organic matter in pelagic sediments of the eastern equatorial Atlantic: suboxic diagenesis. Geochim. Cosmochim. Acta 43, 1075–1090.
Goring-Harford, H.J., Klar, J.K., Pearce, C.R., Connelly, D.P., Achterberg, E.P., James, R. H., 2018. Behaviour of chromium isotopes in the eastern sub-tropical Atlantic Oxygen Minimum Zone. Geochim. Cosmochim. Acta 236, 41–59.
Gueguen, B., Reinhard, C.T., Algeo, T.J., Peterson, L.C., Nielsen, S.G., Wang, X., Rowe, H., Planavsky, N.J., 2016. The chromium isotope composition of reducing and oxic marine sediments. Geochim. Cosmochim. Acta 184, 1–19.
Horner, T.J., Little, S.H., Conway, T.M., Farmer, J.R., Hertzberg, J.E., Janssen, D.J., Lough, A.J.M., McKay, J.L., Tessin, A., Galer, S.J.G., Jaccard, S.L., Lacan, F., Paytan, A., Wuttig, K., 2021. Bioactive Trace Metals and Their Isotopes as Paleoproductivity Proxies: An Assessment Using GEOTRACES-Era Data. Global Biogeochem. Cycles 35, 1–86.
Huang, T., Moos, S.B., Boyle, E.A., 2021. Trivalent chromium isotopes in the eastern tropical North Pacific oxygen-deficient zone. Proc. Natl. Acad. Sci. U. S. A. 118, 1–5.
Huerta-Diaz, M.A., Morse, J.W., 1990. A quantitative method for determination of trace metal concentrations in sedimentary pyrite. Mar. Chem. 29, 119–144.
Huerta-Diaz, M.A., Morse, J.W., 1992. Pyritization of trace metals in anoxic marine sediments. Geochim. Cosmochim. Acta 56, 2681–2702.
Jamieson-Hanes, J.H., Gibson, B.D., Lindsay, M.B.J., Kim, Y., Ptacek, C.J., Blowes, D.W., 2012. Chromium isotope fractionation during reduction of Cr(VI) under saturated flow conditions. Environ. Sci. Technol. 46, 6783–6789.
Janssen, D.J., Rickli, J., Quay, P.D., White, A.E., Nasemann, P., 2020. Biological Control of Chromium Redox and Stable Isotope Composition in the Surface Ocean Global Biogeochemical Cycles. Global Biogeochem. Cycles 34, 1–18.
Janssen, D.J., Rickli, J., Abbott, A.N., Ellwood, M.J., Twining, B.S., Ohnemus, D.C., Nasemann, P., Gilliard, D., Jaccard, S.L., 2021. Release from biogenic particles, benthic fluxes, and deep water circulation control Cr and δ^{53}Cr distributions in the ocean interior. Earth Planet. Sci. Lett. 574, 117163.
Janssen, D.J., Rickl, J., Wille, M., Sepúlveda, S.O., Vogel, H., Dellwig, O., Berg, J.S., Bouffard, D., Lever, M.A., Hassler, C.S., Jaccard, S.L., 2022. Chromium cycling in redox-stratified basins challenges δ^{53}Cr paleoredox proxy applications. Geophys. Res. Lett. 49.
Jeandel, C., Minster, J.F., 1987. Chromium behavior in the ocean: Global versus regional processes. Global Biogeochem. Cycles 1, 131–154.
Joe-Wong, C., Weaver, K.L., Brown, S.T., Maher, K., 2021. Chromium isotope fractionation during reduction of Chromium (VI) by Iron (II/III)-bearing clay minerals. Geochim. Cosmochim. Acta 292, 235–253.
Kim, C., Zhou, Q., Thornton, E.C., Xu, H., 2001. Chromium (VI) Reduction by Hydrogen Sulfide in Aqueous Media: Stoichiometry and Kinetics. Environ. Sci. Technol. 35, 2219–2225.
Kitchen, J.W., Johnson, T.M., Bullen, T.D., Zhu, J., Raddatz, A., 2012. Chromium isotope fractionation factors for reduction of Cr(VI) by aqueous Fe(II) and organic molecules. Geochim. Cosmochim. Acta 89, 190–201.
Koschinsky, A., Hein, J.R., 2003. Uptake of elements from seawater by ferromanganese crusts: Solid-phase associations and seawater speciation. Mar. Geol. 198 (3–4), 331–351.
Lenstra, W.K., Hermans, M., Séguret, M.J.M., Witbaard, R., Severmann, S., Behrends, T., Slomp, C.P., 2020. Coastal hypoxia and eutrophication as key controls on benthic release and water column dynamics of iron and manganese. Limnol. Oceanogr. 66, 807–826.
Li, Y.-H., Gregory, S., 1974. Diffusion of ions in seawater and deep sea sediments. Geochim. Cosmochim. Acta 3 (38), 703–714.
Liu, W., Hao, J., Elzinga, E.J., Piotrowiak, P., Nanda, V., Yee, N., Falkowski, P.G., 2020. Anoxic photogeochemical oxidation of manganese carbonate yields manganese oxide. Proc. Natl. Acad. Sci. U. S. A. 117, 22698–22704.
Lorke, A., Müller, B., Maerki, M., Wüest, A., 2003. Breathing sediments: The control of diffusive transport across the sediment-water interface by periodic boundary-layer turbulence. Limnol. Oceanogr. 48 (6), 2077–2085.
Manceau, A., Charlet, L., Boisset, M.C., Didier, B., Spadini, L., 1992. Sorption and speciation of heavy metals on hydrous Fe and Mn oxides. From microscopic to macroscopic. Appl. Clay Sci. 7, 201–223.
McManus, J., Berelson, W.M., Coale, K.H., Johnson, K.S., Kilgore, T.E., 1997. Phosphorus regeneration in continental margin sediments. Geochim. Cosmochim. Acta 61, 2891–2907.
McManus, J., Berelson, W.M., Klinkhammer, G.P., Hammond, D.E., Holm, C., 2005. Authigenic uranium: Relationship to oxygen penetration depth and organic carbon rain. Geochim. Cosmochim. Acta 69, 95–108.
McManus, J., Berelson, W.M., Severmann, S., Poulson, R.L., Hammond, D.E., Klinkhammer, G.P., Holm, C., 2006a. Molybdenum and uranium geochemistry in continental margin sediments: Paleoproxy potential. Geochim. Cosmochim. Acta 70, 4643–4662.
McManus, J., Berelson, W.M., Severmann, S., Poulson, R.L., Hammond, D.E., Klinkhammer, G.P., Holm, C., 2006b. Molybdenum and uranium geochemistry in continental margin sediments: Paleoproxy potential. Geochim. Cosmochim. Acta 70, 4643–4662.
McManus, J., Berelson, W.M., Severmann, S., Johnson, K.S., Hammond, D.E., Roy, M., Coale, K.H., 2012. Benthic manganese fluxes along the Oregon-California continental shelf and slope. Cont. Shelf Res. 43, 71–85.
Miletto, M., Wang, X., Planavsky, N.J., Luther, G.W., Lyons, T.W., Tebo, B.M., 2021. Marine microbial Mn(II) oxidation mediates Cr(III) oxidation and isotope fractionation. Geochim. Cosmochim. Acta 297, 101–119.
Moos, S.B., Boyle, E.A., 2019. Determination of accurate and precise chromium isotope ratios in seawater samples by MC-ICP-MS illustrated by analysis of SAFe Station in the North Pacific Ocean. Chem. Geol. 511, 481–493.
Moos, S.B., Boyle, E.A., Altabet, M.A., Bourbonnais, A., 2020. Investigating the cycling of chromium in the oxygen deficient waters of the Eastern Tropical North Pacific Ocean and the Santa Barbara Basin using stable isotopes. Mar. Chem. 221, 103756.
Morse, J.W., Luther, G.W., 1999. Chemical influences on trace metal-sulfide interactions in anoxic sediments. Geochim. Cosmochim. Acta 63, 3373–3378.
Muratli, M.J., McManus, J., Mix, A., Chase, Z., 2012. Dissolution of fluoride complexes following microwave-assisted hydrofluoric acid digestion of marine sediments. Talanta 89, 195–200.
Murray, J.W., Spell, B., Paul, B., 1983. The contrasting geochemistry of manganese and chromium in the eastern tropical Pacific Ocean. In: Trace metals in sea water. Springer, Boston, MA, pp. 643–669.
Nasemann, P., Janssen, D.J., Rickli, J., Grasse, P., Frank, M., Jaccard, S.L., 2020. Chromium reduction and associated stable isotope fractionation restricted to anoxic shelf waters in the Peruvian Oxygen Minimum Zone. Geochim. Cosmochim. Acta 285, 207–224.
Neaman, A., Mouélé, F., Trolard, F., Bourrié, G., 2004. Improved methods for selective dissolution of Mn oxides: Applications for studying trace element associations. Appl. Geochem. 19 (6), 973–979.
Olson, S.L., Ostrander, C.M., Gregory, D.D., Roy, M., Anbar, A.D., Lyons, T.W., 2019. Volcanically modulated pyrite burial and ocean–atmosphere oxidation. Earth Planet. Sci. Lett. 506, 417–427.

Pettine, M., Millero, F.J., La Noce, T., 1991. Chromium (III) interactions in seawater through its oxidation kinetics. Mar. Chem. 34, 29–46.
Pettine, M., D'Ottone, L., Campanella, L., Miller, F.J., Passino, R., 1998. The reduction of chromium (VI) by iron (II) in aqueous solutions. Geochim. Cosmochim. Acta 62, 1509–1519.
Pöppelmeier, F., Janssen, D.J., Jaccard, S.L., Stocker, T.F., 2021. Modeling the marine chromium cycle: new constraints on global-scale processes. Biogeosciences 18 (19), 5447–5463.
Poulson, R.L., Siebert, C., McManus, J., Berelson, W.M., 2006. Authigenic molybdenum isotope signatures in marine sediments. Geology 34, 617–620.
Reinhard, C.T., Planavsky, N.J., Robbins, L.J., Partin, C.A., Gill, B.C., Lalonde, S.V., Bekker, A., Konhauser, K.O., Lyons, T.W., 2013. Proterozoic ocean redox and biogeochemical stasis. Proc. Natl. Acad. Sci. USA 110, 5357–5362.
Reinhard, C.T., Planavsky, N.J., Wang, X., Fischer, W.W., Johnson, T.M., Lyons, T.W., 2014. The isotopic composition of authigenic chromium in anoxic marine sediments: A case study from the Cariaco Basin. Earth Planet. Sci. Lett. 407, 9–18.
Rue, E.L., Smith, G.J., Bruland, K.W., 1997. The response of trace element redox couples to suboxic conditions in the water column. Deep-Sea Res. I 44, 113–134.
Sargent, M., Harte, R., Harrington, C., 2002. Guidelines for achieving high accuracy in isotope dilution mass spectrometry (IDMS). The Royal Society of Chemistry, Cambridge.
Scholz, F., Neumann, T., 2007. Trace element diagenesis in pyrite-rich sediments of the Achterwasser lagoon, SW Baltic Sea. Mar. Chem. 107, 516–532.
Scholz, F., Severmann, S., McManus, J., Noffke, A., Lomnitz, U., Hensen, C., 2014. On the isotope composition of reactive iron in marine sediments: Redox shuttle versus early diagenesis. Chem. Geol. 389, 48–59.
Semeniuk, D.M., Maldonado, M.T., Jaccard, S.L., 2016. Chromium uptake and adsorption in marine phytoplankton - Implications for the marine chromium cycle. Geochim. Cosmochim. Acta 184, 41–54.
Shaw, T.J., Gieskes, J.M., Jahnke, R.A., 1990. Early diagenesis in differing depositional environments: The response of transition metals in pore water. Geochim. Cosmochim. Acta 54, 1233–1246.
Sholkovitz, E.R., 1972. The Chemical and Physical Oceanography and the Interstitial Water Chemistry of the Santa Barbara Basin. University of California.
Tang, Y., Webb, S.M., Estes, E.R., Hansel, C.M., 2014. Chromium(III) oxidation by biogenic manganese oxides with varying structural ripening. Environ. Sci. Process Impacts 16, 2127–2136.
van der Weijden, C.H., Reith, M., 1982. Chromium (III) - Chromium (VI) interconversions in seawater. Mar. Chem. 11, 565–572.
Wang, W., Griscom, S.B., Fisher, N.S., 1997. Bioavailability of Cr (III) and Cr (VI) to Marine Mussels from Solute and Particulate Pathways. Environ. Sci. Technol. 31, 603–611.
Wei, W., Frei, R., Chen, T., Klaebe, R., Wei, G., Li, D., Ling, H., 2018. Marine ferromanganese oxide: a potentially important sink of light chromium isotopes? Chem. Geol. 495, 90–103.
Wei, W., Klaebe, R., Ling, H.-F., Huang, F., Frei, R., 2020. Biogeochemical cycle of chromium isotopes at the modern Earth's surface and its applications as a paleo-environment proxy. Chem. Geol. 541, 119570.
Zink, S., Schoenberg, R., Staubwasser, M., 2010. Isotopic fractionation and reaction kinetics between Cr(III) and Cr(VI) in aqueous media. Geochim. Cosmochim. Acta 74, 5729–5745.